Clim. Past Discuss., 10, 3163–3221, 2014
www.clim-past-discuss.net/10/3163/2014/
doi:10.5194/cpd-10-3163-2014

Climate of the Past Discussions
Open Access

Early Paleogene variations in the calcite compensation depth: new constraints using old boreholes across Ninetyeast Ridge in the Indian Ocean

B. S. Slotnick[1], V. Lauretano[2], J. Backman[3], G. R. Dickens[1,3], A. Sluijs[4], and L. Lourens[4]

[1]Department of Earth Sciences, Rice University, Houston, TX 77005, USA
[2]Department of Earth Sciences, Geosciences, Utrecht University, the Netherlands
[3]Department of Geological Sciences, Stockholm University, Stockholm 106 91, Sweden
[4]Department of Earth Sciences, Faculty of Geosciences, Utrecht University, the Netherlands

Received: 25 June 2014 – Accepted: 16 July 2014 – Published: 8 August 2014

Correspondence to: B. S. Slotnick (bss2@rice.edu; bsslotnick@gmail.com)

Published by Copernicus Publications on behalf of the European Geosciences Union.

Abstract

Major variations in global carbon cycling occurred between 62 and 48 Ma. To better constrain the cause and magnitude of these changes, the community needs early Paleogene carbon isotope and carbonate accumulation records from widely separated deep-sea sediment sections, especially including the Indian Ocean. With the potential for renewed scientific drilling in the Indian Ocean, we examine lithologic, nannofossil assemblage, carbon isotope, and carbonate content records for late Paleocene – early Eocene sediment recovered at three existing sites spanning Ninetyeast Ridge: Deep Sea Drilling Project (DSDP) Sites 213 (deep, east), 214 (shallow, central), and 215 (deep, west). The sediment sections are not ideal, because they were recovered in single holes using rotary coring methods. Site 214 was very shallow during the late Paleocene, when it received significant amounts of neritic carbonate. The δ^{13}C records at Sites 213 and 215 are similar to those generated at several locations in the Atlantic and Pacific. The prominent high in δ^{13}C across the Paleocene carbon isotope maximum (PCIM) occurs at Site 215, and the prominent low in δ^{13}C across the early Eocene Climatic Optimum (EECO) occurs at both Site 213 and Site 215. The Paleocene–Eocene thermal maximum (PETM) and the K/X event are found at Site 213 but not at Site 215, presumably because of coring gaps. Carbonate content at both Sites 213 and 215 drops to < 5 % shortly after the first occurrence of *Discoaster lodoensis* and the early Eocene rise in δ^{13}C (~ 52 Ma). This reflects a rapid shoaling of the calcite compensation depth (CCD), and likely a major decrease in the net flux of ^{13}C-depleted carbon to the ocean. Our work further constrains knowledge of the early Paleogene CCD, but more importantly suggests that excellent early Paleogene carbonate accumulation records might be recovered from the central Indian Ocean with future scientific drilling.

CPD
10, 3163–3221, 2014

1 Introduction

Pronounced changes in global carbon cycling characterize a 14 Myr window of the early Paleogene from 62 to 48 Ma. As perhaps best expressed in stable carbon isotope records of marine carbonate (Shackleton, 1986; Zachos et al., 2001, 2010; Slotnick et al., 2012), large magnitude δ^{13}C perturbations span both long (> 1 Myr) and short (< 0.2 Myr) time intervals (Fig. 1). A prominent rise in δ^{13}C begins ca. 62 Ma and reaches a Cenozoic high ca. 58 Ma. From this Paleocene carbon isotope maximum (PCIM), δ^{13}C drops over ~ 5 Myr, culminating in a minimum near the start of the early Eocene Climatic Optimum (EECO) ca. 53 Ma. The δ^{13}C rises over the next 4 Myr, such that values at 49 Ma are nearly the same as at 62 Ma. Superimposed on this major oscillation were several brief carbon isotope excursions (CIEs), when the δ^{13}C decreased significantly within 10 to 50 ka, and recovered within another 50 to 200 kyr (Cramer et al., 2003; Nicolo et al., 2007; Galeotti et al., 2010; Stap et al., 2010). The Paleocene–Eocene thermal maximum (PETM) ca. 56 Ma (Westerhold and Röhl, 2009; Charles et al., 2011), represents the extreme case (e.g., Kennett and Stott, 1991; Sluijs et al., 2007). Throughout this work, we follow the astronomically tuned "Option-1" early Paleogene time scale of Westerhold et al. (2008) for ease of reference and comparison to other data sets (Table 1), although this has been argued to be offset by one 400 kyr eccentricity cycle near the late Paleocene (Hilgen et al., 2010; Vandenberghe et al., 2012).

Both the long-term and short-term δ^{13}C perturbations (Fig. 1) have been attributed to major changes in organic carbon fluxes to and from the ocean–atmosphere system (Shackleton, 1986; Dickens et al., 1995; Kurtz et al., 2003; Sluijs et al., 2007; Komar et al., 2013). The rises in δ^{13}C toward the PCIM and after the EECO reflect net removal of ^{13}C-depleted carbon, the drop in δ^{13}C toward the EECO represents net addition of ^{13}C-depleted carbon; the CIEs, in turn, mark abrupt injections of ^{13}C-depleted carbon followed by partial sequestration. However, controversy surrounds the cause and

CPD
10, 3163–3221, 2014

magnitude of these carbon flux changes because they are difficult to reconcile with conventional models of global carbon cycling (e.g., Dickens, 2003; Komar et al., 2013).

Records of deep-sea carbonate accumulation may constrain perspectives of early Paleogene carbon cycling considerably (Dickens et al., 1997; Zeebe et al., 2009; Leon-Rodriguez and Dickens, 2010; Cui et al., 2011; Komar et al., 2013). Calcite solubility in the deep ocean generally increases with depth, principally because of greater pressure. At constant calcium ion concentrations [Ca^{2+}], higher carbonate ion concentrations [CO_3^{2-}] are therefore necessary to maintain calcite saturation. By contrast, [CO_3^{2-}] generally decreases with depth. The combination of both factors leads to depth horizons in the ocean that impact calcite preservation on the seafloor (e.g., Broecker and Peng, 1982; Boudreau et al., 2010). From the perspective of the sedimentary record, the lysocline is where calcite dissolution first becomes apparent (Kennett, 1982), while the calcite compensation depth (CCD) is where calcite dissolution balances "calcite rain" from above. Although both terms come with caveats (Boudreau et al., 2010), the CCD generally lies hundreds of meters below the lysocline. For this study, we equate the CCD to where the weight percent of $CaCO_3$ drops below < 10 % due to dissolution (Broecker, 2008; Boudreau et al., 2010).

On long-time frames, [CO_3^{2-}] relates to the total mass of carbon in the ocean (Zeebe and Westbroek, 2003). The long-term rises and drops in $\delta^{13}C$ across the early Paleogene should therefore respectively coincide with slow shoaling and slow deepening of the lysocline and CCD (Hancock et al., 2007; Kump et al., 2009; Komar et al., 2013). The CIEs should manifest as rapid rises in the lysocline and CCD, followed by rapid falls, the latter sometimes represented by excess calcite accumulation, coined "carbonate overcompensation" (e.g., Dickens et al., 1997; Zachos et al., 2005; Leon-Rodriquez and Dickens, 2010; Kelly et al., 2010). Crucially, on both long and short time frames, the magnitude of such changes should relate to amounts of carbon added to or removed from the ocean and atmosphere (Dickens et al., 1997; Cui et al., 2011; Komar et al., 2013). Early work regarding Cenozoic evolution of the CCD (Berger, 1972; van Andel, 1975) indicated limited variation during the early Paleogene. However, more

CPD
10, 3163–3221, 2014

recent records support significant changes in carbonate accumulation over this time, indicating a dynamic CCD on the million-year time scale (e.g., Rea and Lyle, 2005; Leon-Rodriguez and Dickens, 2010; Pälike et al., 2012), as well as across some of the CIEs (e.g., Zachos et al., 2005; Stap et al., 2009; Cui et al., 2011).

The long-term CCD record between 62 and 52 Ma remains poorly constrained (Pälike et al., 2012), especially for the Indian Ocean. Moreover, CCD records prior to 52 Ma have not been tightly coupled to δ^{13}C records. In this study, we aim to (1) generate early Paleogene carbonate content and δ^{13}C records at three existing Deep Sea Drilling Project (DSDP) sites in the Indian Ocean, (2) examine these records with current perspectives for global carbon cycling between 62 and 48 Ma, and (3) establish whether better records might be collected with future drilling.

2 The Central Indian Ocean and DSDP Leg 22

2.1 Bathymetry and basement origin

Three large-scale features characterize the bathymetry of the central Indian Ocean, loosely defined as the region between 5° S and 15° S latitude and 75° E and 100° E longitude (Fig. 2). In the middle lies the north-south oriented Ninetyeast Ridge. This ~ 4600 km long (from ~ 10° N to ~ 31° S) parapet separates two abyssal plain regions: Wharton Basin and Cocos Basin to the east, and Mid-Indian Basin to the west. The ridge was generated by "hotspot volcanism" as the Indo-Australian Plate moved north over the Kerguelen plume; ages of basalt along the ridge systematically become younger to the south (Fig. 2) (Saunders et al., 1991; Frey et al., 2011).

The surrounding plains are floored by oceanic crust formed along the South Eastern Indian Ridge (SEIR) and Central Indian Ridge (CIR) during the late Cretaceous through middle Paleogene, as indicated by tholeiitic basalt recovered and dated at several DSDP sites (Frey et al., 1977). Reconstructing paleo-positions in these low lying abyssal plains is complicated because of broad diffusive plate boundaries, and

CPD
10, 3163–3221, 2014

because of multiple stages of rotation throughout much of the Cenozoic (Patriat and Achacha, 1984; Cande et al., 2010). Nonetheless, ages of basalt throughout the plains and basins surrounding Ninetyeast Ridge generally become younger to the south (Fig. 2).

2.2 Sites 213, 214, and 215

This study focuses on three Deep Sea Drilling Project (DSDP; Leg 22) sites straddling Ninetyeast Ridge (von der Borch and Sclater, 1974; Fig. 2). Site 213 is located ~ 500 km east of Ninetyeast ridge at 10°12.71′ S, 93°53.77′ E, and 5601 m below sea level (m b.s.l.). Site 214 lies on the crest of Ninetyeast Ridge at 11°20.21′ S, 88°43.08′ E, and 1655 m b.s.l.. Site 215 is located ~ 300 km west of Ninetyeast Ridge at 8°07.30′ S, 86°47.50′ E, and 5309 m b.s.l..

All three sites cored basalt of early Paleogene age (Fig. 2). Igneous basement is approximately 56, 62, and 59 Ma at Sites 213, 214 and 215, respectively (MacDougall, 1977; Peirce, 1978; Frey et al., 2011). Given the tectonic history for the region, all three sites were located further south and in shallower water during the early Paleogene. Plate reconstructions have the sites at ~ 30° S in the late Paleocene (ODSN 2011). Sites 213 and 215 were located at the SEIR crest at the time of basalt emplacement, presumably ~ 2.75 km below sea level. Site 214 was near or above the sea surface until 61 Ma. Lowermost sediment recovered at Site 214 contains glauconitic silt with gastropods and bivalves, as well as lignite and tuff.

Coring operations recovered 139 m of pelagic sediment at Site 213, 311 m of pelagic sediment and 35 m of neritic sediment at Site 214 (excluding lowermost volcaniclastic material), and 113 m of pelagic sediment at Site 215 (von der Borch and Sclater, 1974). Sediment age was determined primarily through calcareous biostratigraphy. This study focuses on cores containing upper Paleocene and lower to middle Eocene sediment (Figs. 3–6). Studied intervals comprise a range of lithologies, but especially nannofossil ooze and clay. Of primary interest are occasional clay-rich horizons within nannofossil

CPD
10, 3163–3221, 2014

ooze, and major shifts from nannofossil ooze to clay, such as within lower Eocene sediment at Site 213 (Core 14) and at Site 215 (Core 9).

2.3 Previous work on early Paleogene sequences

Previous investigations of lower Paleogene sediment at Sites 213, 214, and 215 (von der Borch and Sclater, 1974; McGowran, 1974; Gartner, 1974; Bukry, 1974; Hovan and Rea, 1992; Zachos et al., 1992; Berggren and Norris, 1997; Ravizza et al., 2001; Tremolada and Bralower, 2004) offer age constraints. Much of this work concerns nannofossil and foraminiferal biostratigraphy. Previous investigations were conducted at low depth resolution, except for work across the PETM at Site 213 (Ravizza et al., 2001; Tremolada and Bralower, 2004). Most of the earlier work is not on a common and current early Paleogene time scale, and needs amendment for comparison to other locations.

3 Methods

3.1 Stratigraphic log and samples

In contrast to most paleoceanographic expeditions over the last two decades, only one hole was drilled at each site. Furthermore, drilling employed rotary coring methods (Storms, 1990). The combination almost necessarily implies discontinuous sedimentary records that contain disturbed intervals. This is partly confirmed for the sites of interest through photographs and logs, which show some highly disturbed intervals (Fig. 7), and numerous cores less than 9.5 m in length, even though drilling generally advanced by this amount (von der Borch and Sclater, 1974). More problematic are potential core gaps that may exist between successive cores (Ruddiman et al., 1987; Hagelberg et al., 1992; Dickens and Backman, 2013). As discovered on drilling expeditions circa 1985–1987, typically about 1 m (but up to 3 m) may be missing between

CPD
10, 3163–3221, 2014

successive hydraulic piston cores. We assume this also occurs between successive rotary cores in unlithified ooze and clay, such as at Sites 213, 214, and 215. We therefore have recast original depths and placement of cores on a meters composite depth (mcd) scale. Missing core sections are consistently placed at the bottom of cores, and gaps between successive cores were assumed to be 1 m (Figs. 3–6 and 8–10). Obviously, the length of core gaps is arbitrary, but the inclusion of such gaps shows expected locations of missing sediment.

A total of 395 early Paleogene sediment samples were taken from Sites 213, 214, and 215. Individual samples were 10 cm^3 in size, and taken using a plastic scoop.

3.2 Sample preparation

Each sample was freeze-dried, and split into two aliquots: one for nannofossil examination, the other for geochemistry. The geochemistry aliquot was ground and homogenized using a glass mortar and pestle. Ground material of each sample was placed into a tube with 18 MΩ deionized water, mixed using a mini vortexer, and centrifuged for 10, 15, and 25 min sequentially to remove dissolved ions. Water was decanted after each interval of centrifuging. Centrifuged sample aliquots then were freeze-dried a second time.

3.3 Nannofossil assemblages

Calcareous nannofossils were investigated in 62 samples to refine ages. Smear slides were made following standard methods. Estimates of abundance and preservation follow the guidelines outlined by Pälike et al. (2010). For the abundance of total nannofossils: D = dominant (> 90 % of total sediment grains); A = abundant (50–90 %): C = common (10–50 %); F = few (1–10 %); R = rare (< 1 %); B = barren. For the preservation of nannofossils: G = good (little evidence of dissolution or recrystallization, primary morphological characteristics only slightly altered, specimens identifiable to the species level); M = moderate (specimens exhibit some etching or recrystallization, pri-

CPD
10, 3163–3221, 2014

mary morphological characteristics somewhat altered, most specimens identifiable to the species level); P = poor (specimens severely etched or overgrown, primary morphological characteristics largely destroyed, fragmentation has occurred, specimens often not identifiable at the species or genus level).

A well-established sequence of appearances and disappearances of calcareous nannofossil species and genera spans the early Paleogene. These biohorizons have been calibrated to magneto- and/or cyclostratigraphy. We use the NP zonal scheme of Martini (1971). Some species, for example *Discoaster lodoensis*, have a pulsed onset at some sites (Agnini et al., 2007; Dickens and Backman, 2013). As such, there is a true base (B) as well as a higher position when the species begins to occur consistently and with higher relative abundances (Base common, or Bc).

3.4 Geochemistry

Dried splits of bulk sediment samples were analyzed for carbonate content and stable isotope ratios at Utrecht University. Carbonate content was determined from the amount of carbon dioxide generated during combustion using a LECO SC-632 analyzer. Each sample was weighed, and calculations incorporated these masses. Multiple analyses of the WEPAL-ISE 983 and in-house carbonate standards form the basis for accuracy and precision (0.8 % at 1σ). Stable carbon and oxygen isotopes were determined using an ISOCARB common acid bath carbonate preparation device linked to a VG24 SIRA mass spectrometer. Instrumental calibrations were constrained using in-house standards IAEA-CO-1 and NAXOS (Coplen et al., 2006). Ratios were converted to standard delta notation relative to Vienna Pee Dee Belemnite (vPDB). Analytical precision was 0.05 ‰ at 1σ and 0.10 ‰ at 2σ for δ^{13}C and δ^{18}O, respectively. Although all samples were analyzed for stable isotopes, some samples with very low (< 5 %) carbonate contents did not give accurate values.

CPD
10, 3163–3221, 2014

4 Results

4.1 Nannofossil assemblages and age control

The intervals investigated span the Paleocene/Eocene boundary, from Zone NP10 to Zone NP12 (Site 213), Zone NP4-5 to Zone NP12 (Site 214) and Zone NP7-8 to Zone NP12 (Site 215) in the biozonation of Martini (1971). The Paleocene/Eocene boundary, however, is lost in core gaps at all three sites. These sites were originally investigated by Gartner (1974) and Bukry (1974). The data produced here is consistent with their findings. Assemblages are mostly poorly preserved (Tables 2–4).

Based on presence and absence of assemblage components, a minimum and maximum age can be assigned to each sample. Age estimates are from Agnini et al. (2006, 2007), placed on an updated time scale (Option 1, Westerhold et al., 2008; Table 1).

The following biochronologic criteria were used for determining age relationships at Site 213. A sample showing an overlap in the ranges of *Tribrachiatus orthostylus* and *Discoaster lodoensis* indicates that the sample must be older than 50.70 Ma, which is the estimate for the disappearance, or top, of *T. orthostylus*. This estimate thus represents the youngest possible (mininum) age for the sample. Similarly, the oldest possible age for the sample must be the appearance, or base, of *D. lodoensis*, occurring at 53.24 Ma. The overlap between these taxa indicate Zone NP12.

Samples below the range of *D. lodoensis* and showing presence of *Sphenolithus radians* indicate Zone NP 11, and a minimum age of 53.24 (sample older than base *D. lodoensis*) and a maximum age of 53.85 Ma (sample is younger than appearance age of *S. radians*). Samples below the range of *T. orthostylus* and showing presence of *Discoaster diastypus* indicate Zone NP10, a minimum age of 54.00 Ma (sample is older than the appearance age of *T. orthostylus*) and a maximum age of 54.48 Ma (sample is younger than the appearance age of *D. diastypus*). Samples showing an overlap in range between *Zygrhablithus bijugatus* and *Fasciculithus tympaniformis*, and in which the former dominates in abundance over the latter, range in age from 55.11 Ma (sample is older, minimum age, than the top of *F. tympaniformis*) to 55.47 Ma (sample

CPD
10, 3163–3221, 2014

is younger, maximum age, than the cross-over in abundance between *F. tympaniformis* and *Z. bijugatus*).

Gartner (1974) has marked an overlap in range between *Ericsonia robusta* and *Discoaster multiradiatus* in Sample 213-17-1, 120 cm, indicating Zone NP9 and an age range from 56.66 Ma (top *E. robusta*) to 56.76 Ma (base *D. multiradiatus*). This implies that the Paleocene/Eocene boundary is lost in the gap between Cores 213-16 and 213-17.

Several of these criteria were used also at Site 214. The overlap in range between *D. lodoensis* and *S. radians* (53.24–53.85 Ma) occurs in a single sample (214-35-4, 140–142 cm). The next deeper sample (214-36-2, 120–122 cm) holds an upper Paleocene assemblage including *Heliolithus kleinpellii*. The appearance of this species defines the base of Zone NP6 (59.02 Ma), and disappears at 58.33 Ma in the lowermost part of Zone NP7. Absence of *H. kleinpellii* and presence *of Heliolithus cantabriae* suggests an age range of 59.02 Ma (older than base *H. kleinpellii*) to 59.37 Ma (younger than base *H. cantabriae*) and Zone NP5. The base of *Fasciculithus tympaniformis* at 60.90 Ma defines base Zone NP5. Absence of *H. cantabriae* and presence of *F. tympaniformis* indicates an age range from 59.37 Ma (older than, minimum age, base *H. cantabriae*) to 60.90 Ma (younger than, maximum age, base *F. tympaniformis*). Preservation is too poor in lower Core 214-38 and Core 214-39 to judge whether or not *F. tympaniformis* is present. However, rare *Fasciculithus* spp. were present, indicating an age range from 59.37 Ma (older than base *H. cantabriae*) to 61.21 Ma (younger than base *Fasciculithus* spp.).

Site 214 has a hiatus encompassing, at least, the interval from 53.85 Ma to 58.33 Ma.

Criteria used to provide age ranges of samples in Site 215 are as above in the NP10 through NP12 interval. The Paleocene/Eocene boundary is lost in the gap between Cores 215-11 and 215-12. Diverse and abundant *Fasciculithus* spp. indicate an age older (minimum) than 55.47 Ma. Absence of *E. robusta* indicates an age younger than (maximum) than 56.66 Ma. Overlap in the ranges between *E. robusta* and *Discoaster multiradiatus* indicates a minimum age of 56.66 Ma (top *E. robusta*) and a maximum

CPD
10, 3163–3221, 2014

age of 56.76 Ma (base *D. multiradiatus*). The latter event defines the base of Zone NP9. Absence of *D. multiradiatus* and presence of *E. robusta* indicates a minimum age of 56.76 Ma (base *D. multiradiatus*) and a maximum age of 57.04 Ma (base *E. robusta*). This composition suggests Zone NP7-8. Absence of *E. robusta* and presence of *Discoaster mohleri* indicates a minimum age of 57.04 Ma (base *E. robusta*) and a maximum age of 58.55 Ma (base *D. mohleri*).

4.2 Carbonate content

Carbonate content measurements at Site 213 (Table 5) render a complex curve (Fig. 8). Values are < 2 % and average 1 % from the top of section 13-1 through the bottom of section 14-4 (113.8–129.8 mcd). Starting near the top of section 14-5, carbonate contents increase significantly, reaching 73 % by 132.8 mcd. A prominent low in carbonate content, where values drop to about 2 % marks the top of Core 15 (134.5–135.5 mcd). Over the next 7.6 m, carbonate content generally increases, although with two short intervals of relatively low values, centered at 135.6 mcd and 139.5 mcd. From 139.9 mcd to 149.3 mcd, carbonate content is generally high, ranging between 85 to 91 %. Importantly, moderate nannofossil preservation spans this interval of high carbonate content. The core-catcher of section 16 has very low carbonate content.

Carbonate content data at Site 214 (Table 6) also lead to a complex profile (Fig. 9). Values are > 91 % and average 93 % from the top of section 34-1 through the top of section 35-1 (314.6–324.5 mcd). Starting near the top of section 35-1, carbonate contents decrease slightly, reaching 85 % by 329.6 mcd. A further decrease in carbonate contents spans the base of sections 35-4 and 35-cc, where values drop to 74 % at 330.7 mcd. Beginning at 336.1 mcd and for the next 34.7 m downcore, carbonate contents generally fluctuate between 4 and 65 %, and average 37 %.

Carbonate content measurements at Site 215 (Table 7) contrast with the other two sites: except for a transition interval, they are either very low or very high, depending on depth (Fig. 10). Values are < 3 % and average 1 % from the top of section 8-1 through the middle of section 9-3 (65.4–78.6 mcd). Starting in section 9-3, carbonate contents

CPD
10, 3163–3221, 2014

increase significantly reaching 93 % by 87.9 mcd. Over the next 48.5 m, carbonate content is universally high, ranging between 82 and 97 %. As at Site 213, moderate nannofossil preservation spans the interval of particularly high carbonate content, although in general, carbonate content at Site 215 is higher than at Site 213. The lowest values within this interval are centered at 119.6 mcd.

Prior to our work, several analyses of carbonate content were conducted at these sites as part of DSDP Leg 22 operations (Pimm, 1974). Most samples from the two studies appear to be within 5 % (Figs. 8–10), although a rigorous comparison cannot be made because of slight differences in depth between samples.

4.3 Carbon isotopes

Bulk carbonate δ^{13}C values at Site 213 (Table 5) lead to a complicated profile (Fig. 8). Samples at the top of the studied section (113.8–130.1 mcd) have too little carbonate for reliable stable isotope analyses. From the top of section 14-5 through the base of section 14-6 (130.1–132.8 mcd), values range between 1.50 and 2.18 ‰ and average 1.87 ‰. A prominent low in bulk carbonate δ^{13}C, with values reaching 1.17 ‰, marks the top of Core 15 (134.7–135.3 mcd). Over the next 3.8 m, bulk carbonate δ^{13}C generally decreases, culminating in a pronounced low between 139.1 and 139.8 mcd. This is followed below by a general rise through the base of section 15-6. From 145.8 to 149.5 mcd, bulk carbonate δ^{13}C is generally high, but decreases gradually from 2.27 to 2.02 ‰. This drop in δ^{13}C intensifies through sections 16-4 and 16-cc, as also found by Ravizza et al. (2001), such that a prominent negative CIE of at least 1.4 ‰ exists.

Bulk carbonate δ^{13}C values at Site 214 (Table 6) generally decrease with greater depth (Fig. 9). However, the low δ^{13}C values measured in cores 36 through 39-3 are noteworthy, because they cannot represent primary pelagic carbonate. These samples accumulated during the middle Paleocene (as some contain *H. kleinpellii* or *H. cantabriae*), but clearly contrast with the δ^{13}C composition of pelagic carbonate from this time interval. The anomalous δ^{13}C may be consistent with neritic carbonate. Shallow marine carbonate exhibits a wide range in δ^{13}C composition (cf. Swart and Eberli,

CPD
10, 3163–3221, 2014

2005), and can be significantly depleted in ^{13}C when they precipitate in exchange with pore waters having a high contribution of ΣCO_2 from organic carbon respiration (Patterson and Walter, 1994a, 1994b; Sanders, 2003). We have not investigated this possibility further, but the interval at Site 214 provides an interesting example of where carbon isotope stratigraphy does not work.

Bulk carbonate $\delta^{13}C$ measurements at Site 215 (Table 7) give a fairly straightforward curve (Fig. 10). As at Site 213, uppermost samples (65.4 to 78.6 mcd) contain too little carbonate to yield reliable bulk carbonate $\delta^{13}C$ values. Near the base of section 9-3, values range between 1.71 and 2.03 ‰. Values then drop to 1.08 ‰ at the top of section 10-1. Over the next 28.8 m, bulk carbonate $\delta^{13}C$ generally rises, reaching ~ 3.5 ‰ in the base of section 12-6 (115.4 mcd). From 118.2 to 136.4 mcd, bulk carbonate $\delta^{13}C$ is generally high. Except for a few relatively slight drops in $\delta^{13}C$, one located within section 13-2, from 119.1–119.6 mcd, values exceed 3 ‰ in lower cores at Site 215.

4.4 Oxygen isotopes

Bulk carbonate $\delta^{18}O$ measurements at Sites 213, 214, and 215 (Tables 5–7) lead to curves with some noteworthy observations (Figs. 8–10). At Site 213, from the top of section 14-5 to the base of section 15-6, values vary between −2.49 and −0.76 ‰ with considerable scatter. Below, bulk carbonate $\delta^{18}O$ rises slightly from ~ −1.2 to ~ −0.6 ‰, and then drops significantly, reaching −1.89 ‰ at 157.7 mcd. At Site 214, values range between −1.52 and 0.11 ‰, and generally decrease with depth. At Site 215, values vary between −2.09 and 1.31 ‰ with no discernible trend.

CPD
10, 3163–3221, 2014

5 Discussion

5.1 Overview

The reconstruction of a "paleo-CCD curve" for an ocean basin requires key information from multiple sites (e.g., van Andel, 1975; Pälike et al., 2012). At a given site, these are: (1) the age of the sediment deposited, (2) the depth trajectory through time, and (3) the carbonate accumulation overlain upon this trajectory.

5.2 Revised age models

Our nannofossil assemblage data provide internally consistent age constraints at all three sites. Although moderate to poor preservation impacts precise placement of key nannofossil datums (tops and bases of index species), depth horizons can be assigned age ranges (Figs. 4–6). These ranges result in age-depth curves that generally conform to previous work (Figs. 8–10), once absolute ages for various datums in older literature have been placed onto a current time-scale (Table 1). This includes work on calcareous nannofossils (Gartner, 1974; Tremolada and Bralower, 2004) and on foraminifera (McGowran, 1974; Berggren and Norris, 1997; Hovan and Rea, 1992).

Characteristic features of early Paleogene $\delta^{13}C$ curves can be used for stratigraphic purposes (e.g., Shackleton, 1986; Slotnick et al., 2012). Although the $\delta^{13}C$ records at Sites 213, 214 and 215 are not ideal, because of core gaps, drilling disturbance and hiatuses, key features can be identified. The prominent high in $\delta^{13}C$ during the PCIM and the subsequent 5 Myr decrease in $\delta^{13}C$ toward the EECO is found at Site 215. The $\delta^{13}C$ rise during and following the EECO is found at Site 214. At least two short-term CIEs can be found at Site 213. Indeed, once the $\delta^{13}C$ records at the three sites are spliced together in the time domain, and once intervals of missing sediment are accounted for, a fairly reasonable correlation to other marine $\delta^{13}C$ records emerges (Fig. 11).

CPD
10, 3163–3221, 2014

5.3 Site subsidence trajectories

The water depth of tholeiitic basalt formed at a mid-ocean ridge younger than 70 Ma can be predicted using subsidence curves (Sclater et al., 1971; Berger, 1972; van Andel, 1975). For Sites 213 and 215, basalt emplacement clearly occurred at a ridge axis < 70 Ma (most likely the SEIR), a fact substantiated by metalliferous ooze mixed with pelagic calcareous organisms in basal sediments (von der Borch and Sclater, 1974). A generic subsidence equation for such sites is (Parsons and Sclater, 1977):

$$z = z_{(o)} + Ct^{1/2}, \quad (1)$$

where z is the present water depth (m b.s.l.), $z_{(o)}$ is depth of the ridge at initial time (m b.s.l.), C is the subsidence rate (m Myr^{-1}), and t is time since formation (Ma). Because porous sediment adds mass on top of the basalt but is about half the density, it should be accounted for (Rea and Lyle, 2005). A simple correction is (Berger, 1973; Rea and Lyle, 2005):

$$z = (z_{(o)} + Ct^{1/2}) - 0.5z_{(s)}, \quad (2)$$

where $z_{(s)}$ is the thickness of overlying sediment (m).

As noted for CCD reconstructions in the Eastern Pacific (Leon-Rodriguez and Dickens, 2010; Pälike et al., 2012), two problems confront such depth reconstructions. First, water depths range significantly along the crest of modern mid-ocean ridges (e.g., Cochran, 1986; Calcagno and Cazenave, 1994). For the crest of the modern SEIR, they range from 2500 to 3300 m b.s.l., and generally deepen to the southeast (Cochran, 1986; Mahoney et al., 2002). This range of "zero-age" depths probably reflects differences in mantle properties below the ridge crest, perhaps including a drop in upper mantle temperatures to the east (Cochran, 1986; Klein et al., 1991; Mahoney et al., 2002). Second, subsidence rates along mid-ocean ridges vary significantly (e.g., Cochran, 1986; Calcagno and Cazenave, 1994). For the SEIR, they vary from 200–460 m Myr$^{-1/2}$, with some of this variance related to the presence of fracture zones

CPD
10, 3163–3221, 2014

(Cochran, 1986). Together, these heterogeneities add uncertainty to subsidence curve estimates (Leon-Rodriguez and Dickens, 2010). It is important to recognize, though, that the maximum uncertainty in past depth generally occurs when the site is at or near the ridge crest, because subsidence decays exponentially over time (Eq. 1).

When discussing crustal subsidence in the southern Indian Ocean, Cochran (1986) noted a generally symmetric bathymetric profile along the SEIR between 90° and 96° E latitude. He further suggested a subsidence rate of 363 m $Myr^{-1/2}$ for the north flank, which is comparable to the average for mid ocean ridges (Parsons and Sclater, 1977). This information, along with an average ridge crest depth (2750 m), can be used as a starting point for Sites 213 and 215, such that:

$$z = (2750 + 363t^{1/2}) - 0.5z_{(s)}. \quad (3)$$

If seafloor depths at Sites 213 and 215 adhered to Eq. (3), they should now lie at 5391 m b.s.l. (Site 213) and 5463 m b.s.l. (Site 215). The predicted depths are close, but slightly off from actual depths (−210 m, Site 213; +154 m, Site 215). Previous work regarding subsidence at Sites 213 and 215 (van Andel, 1975) recognized this discrepancy, and thus gave different and deeper starting depths for Site 213 (~ 3300 m b.s.l.) and Site 215 (~ 3100 m b.s.l.). These alternative "zero-age" depths imply slower subsidence rates, and ultimately deeper depth trajectories for both sites. There is no simple means to arrive at the correct depth trajectories over time, and different age/depth points along plausible curves should be taken as a reflection of uncertainty. For Sites 213 and 215, absolute depths for the early Paleogene may be off by 300–600 m, depending on time since basalt emplacement. We do note, though, that at Sites 213 and 215, inclusion of the thin sedimentary packages (~ 150 m) has minimal impact on the subsidence curve.

Site 214 on the crest of Ninetyeast Ridge has a much different depth trajectory than that at Sites 213 and 215. Aseismic ridges subside following the underlying plate as cooling and contraction progress, and at rates proportional to the square root of age (Detrick et al., 1977). However, if crustal age is significantly older than the hot spot (arbi-

CPD
10, 3163–3221, 2014

trarily set at 3 Myr at Site 214), cooling and contraction already will have initiated, which should result in slower subsidence (Detrick et al., 1977). For Site 214, we set a starting "depth" at 50 m above sea level (a.s.l.), a height broadly consistent with lignites and volcaniclastics in lowermost cores, and neritic carbonate in subsequent cores. Thus, portions of Ninetyeast Ridge were once emergent volcanic islands, a concept inferred by others (Saunders et al., 1991; Frey et al., 1991; Carpenter et al., 2010). Using this starting height, we forced the subsidence (286 m $Myr^{-1/2}$) so the location of Site 214 slowly sank to 600 m b.s.l. by 48 Ma, and to 1655 m b.s.l. at present-day.

As an aside, the significant and unexpected hiatus we document at Site 214 might be explained in multiple ways. The location could have been in shallow water (< 500 m b.s.l.) between 58.33 and 53.85 Ma, and continually swept clean of sediment. Alternatively, it could represent a time of temporary uplift of underlying oceanic crust through compression (McKenzie and Sclater, 1971).

5.4 CCD reconstruction for the early Paleogene central Indian Ocean

The above age constraints and subsidence models permit records of carbonate content to be placed over time and depth in an effort to reconstruct the CCD (Fig. 11). As noted previously, the carbonate records at Site 214 generally can be ignored for this exercise, because to the site was always much shallower than the CCD. However, the carbonate records at Sites 213 and 215 provide important information.

High carbonate contents, typically exceeding 80 %, characterize sediment over most of the lower portion of studied intervals at Site 213 and 215. For much of the late Paleocene and early Eocene, more specifically from 59 through 51 Ma, the CCD was significantly deeper than these locations. However, at both locations, carbonate contents dropped precipitously (to < 5 %) within calcareous nannofossil zone NP12. We strongly suggest this transition from carbonate ooze to clay corresponds to a rapid rise in the CCD, which occurred between 52 and 50 Ma.

CPD
10, 3163–3221, 2014

Moderate preservation of nannofossils spans most of the interval of high carbonate content at Sites 213 and 215. This observation suggests dissolution of microfossil assemblages, albeit relatively minor, and a seafloor location at or just below the lysocline. Such a setting would be expected along flanks of mid-ocean ridges, even in the earliest Eocene, as carbonate saturation horizons were probably shallower than at present-day (van Andel, 1975; Leon-Rodriguez and Dickens, 2010). Prior to the major drop in carbonate content and near the NP10/NP11 zonal boundary (i.e., about 54 Ma), preservation of nannofossils becomes poor at both Sites 213 and 215 (Tables 5, 7). This suggests the sites were further below the lysocline, either through subsidence or the rising of carbonate saturation horizons.

The generally lower carbonate contents at Site 213 compared to those at Site 215 requires explanation. This is because, with a standard crustal subsidence model, Site 213 should have been shallower than Site 215, especially during the early Paleogene (Fig. 11), and consequently should have better carbonate preservation. An obvious possibility is that crustal depths at time zero ($z_{(o)}$, Eq. 1) were significantly different, and Site 213 was deeper than Site 215 by several hundred meters (van Andel, 1975). An intriguing alternative is that a very shallow Ninetyeast Ridge, as exemplified by the sediment record at Site 214, impeded east–west flow of water at intermediate to deep ocean depths. More specifically, the CCD may have been shallower east of Ninetyeast Ridge for much of the early Paleogene.

Five brief drops in carbonate content span the thick interval of high carbonate at Site 213 (Fig. 8). Based on nannofossil datums and $\delta^{13}C$ measurements, these carbonate lows probably correspond to known hyperthermal events. From bottom to top, the first carbonate low (to 3 %) occurs within NP10 and marks the PETM. The next three lows (to 40 %, 26 %, 38 %) follow near and above the NP11/12 Zonal boundary. These likely represent some combination of the H, I and J events, as the stratigraphic placement is approximately correct. However, it is difficult to make clear assignment because of major core disturbance. The uppermost carbonate low (to 2 %) lies above the base of *D. lodoensis*, and almost certainly represents the K/X event.

CPD
10, 3163–3221, 2014

The PETM and K/X event at Site 213 warrant special attention, because carbonate contents drop close to zero. This suggests the CCD rose significantly during these hyperthermals, effectively passing above the depth of the location. The high carbonate contents immediately after the events further suggest overshoots, where the CCD dropped to below that before massive carbon injection (e.g., Dickens et al., 1997; Kelly et al., 2012). Presumably similar signals exist at Site 215, but were not recovered because of core gaps.

5.5 Comparison to previous work

The reconstructed late Paleocene-early Eocene CCD for the central Indian Ocean (Fig. 11) is broadly consistent with that determined at several sites in the eastern Indian Ocean (Hancock et al., 2007) and Equatorial Pacific Ocean (Leon-Rodriguez and Dickens, 2010; Pälike et al., 2012) (Fig. 1). In these works, the CCD was relatively deep in the latest Paleocene and earliest Eocene (~ 58 to 52 Ma) but shoaled considerably in the late early Eocene (~ 52 to 50 Ma). The magnitude of this shoaling remains poorly constrained, but probably exceeded several hundreds of meters. Importantly, at Sites 213 and 215 and other locations, the time when the CCD was relatively deep coincided with the long-term early Paleogene drop in $\delta^{13}C$ (Figs. 1 and 11).

Previous reconstructions of the CCD (Berger, 1972; von der Borch and Sclater, 1974; van Andel, 1975; Rea and Lyle, 2005) had this horizon relatively shallow and flat through the early Eocene. This may have resulted from poorly resolved stratigraphy at a few key sites, including Sites 213 and 215. Initial reports of Leg 22 sediment cores identified the early Eocene shift from calcareous ooze to clay, but suggested it happened at Site 215 about 3 Myr after it occurred at Site 213 (MacDougall, 1977; Peirce, 1978). This is not the case because the transition occurred within calcareous biozone NP12 at both sites (Fig. 11). The error seems to have led Gartner (p. 582, 1974) to suggest a significant difference in starting ridge depth ($z_{(o)}$) between the two sites and a stationary CCD across the early Eocene, an interpretation that subsequently became incorporated into early CCD curves (van Andel, 1975).

CPD
10, 3163–3221, 2014

The reconstructed CCD records at Sites 213 and 215 are somewhat similar to that at Site 1215 in the Equatorial Pacific, which drilled into tholeitiic basalt of 58 Ma age. At this location, the PETM and K/X event also are marked by particularly strong carbonate dissolution (Leon-Rodriguez and Dickens, 2010). Interestingly, at Site 1215, a good argument can be made for a long-term deepening of the lysocline beginning around 57 Ma: the site was subsiding rapidly but, excepting hyperthermal events, the preservation of foraminifera tests generally remains similar or improves for several Myr upcore (Leon-Rodriguez and Dickens, 2010). The available carbonate content and preservation records at Sites 213 and 215 neither support nor refute this concept. Site 215 would be helpful in this regard, as the sedimentary record begins at 59 Ma. However, in this discontinuous record, it is not obvious the CCD or lysocline was particularly shallow at 58 Ma, nor that either horizon generally deepened between 58 and 53 Ma. There is only a slight drop in carbonate content between 58 and 57 Ma (section 13-2).

Amongst existing Indian Ocean drill sites, less than 20 contain early Paleogene sediment sequences (Fig. 11). None of these sequences were recovered with multiple drill holes, and are, therefore, discontinuous. Moreover, most of these sequences lack updated and revised stratigraphy, as well as sufficiently resolved carbonate content and stable isotope records. With available data, other locations in the Indian Ocean generally support the CCD record presented here, but also highlight a lack of detail and poor depth constraints.

5.6 Significance toward early Paleogene carbon cycling

Although our latest CCD reconstruction for the Indian Ocean remains poorly defined, the coupled carbonate content and bulk carbonate $\delta^{13}C$ records at Sites 213 and 215 support basic ideas and modeling efforts regarding early Paleogene carbon cycling. In particular and over multiple time scales, the highs and lows in $\delta^{13}C$ seemingly relate to changes in net fluxes of organic carbon to and from the exogenic carbon cycle (e.g., Shackleton, 1986; Dickens et al., 1997; Kurtz et al., 2003; Zeebe et al., 2009; Cui et al., 2011; Komar et al., 2013). Long-term intervals with higher $\delta^{13}C$ should correspond to

CPD
10, 3163–3221, 2014

less carbon in the ocean and atmosphere, and a shallower CCD; the opposite is also true. The CCD defined from records at Sites 213 and 215 generally tracks the $\delta^{13}C$ of bulk carbonate, especially the rise in both records at ~ 52.5 Ma. The short-term CIEs are a different matter, as they represent massive injections of organic carbon, each which should result in a rapid rise in the CCD and lysocline, followed by overcompensation of these horizons. At Site 213, intense dissolution of carbonate occurs across the CIEs, especially the PETM and K/X.

Perhaps the two biggest issues currently confronting the scientific community in regards to early Paleogene carbon cycling are: what are the source or sources of organic carbon behind the long-term and short-term carbon cycle perturbations? Are the long-term and short-term perturbations somehow related? As emphasized by several authors, much can be explained if the shallow geosphere has a large and dynamic organic carbon capacitor (Dickens, 2003; Kurtz et al., 2003; Dickens, 2011; Komar et al., 2013). Effectively, some reservoir connected to the combined ocean–atmosphere–biosphere can store massive amounts of organic carbon over long time intervals, and can return this carbon over both long and short time scales. In theory, potential organic carbon sources can be distinguished with combined records of $\delta^{13}C$ and carbonate saturation horizons (e.g., Dickens et al., 1997; Zeebe et al., 2009; Cui et al., 2011; Komar et al., 2013), because the magnitude of changes in both parameters should relate to variations in carbon mass fluxes.

Even with the additional records presented here, causes for early Paleogene carbon cycle perturbations remain open to interpretation. For example, our Indian Ocean CCD curve can be compared to simulated "long-term" early Paleogene CCD curves predicted for the Atlantic and Pacific oceans (Komar et al., 2013; Fig. 12), which presumably should straddle the response in the Indian Ocean. Whilst changes in the CCD curves have similar timing, they have different magnitudes, by several hundreds of meters. This suggests the overall carbon cycling framework is correct, but either that mass flux variations in the modeling are too small, or that depth constraints on CCD remain

CPD
10, 3163–3221, 2014

poorly characterized. Additional sites drilled on oceanic crust with ages between 75 and 55 Ma are needed to resolve the problem.

5.7 Recommendations for future drilling in the Indian Ocean

The Indian Ocean is particularly relevant to studies of early Paleogene carbon cycling. This is because portions of three mid-ocean ridge segments and several aseismic ridges (e.g., Kerguelen Plateau, Ninetyeast Ridge, Broken Ridge, Chagos-Laccadive Ridge, Mascarene Plateau) are underlain by basalt of late Cretaceous or Paleocene age (i.e., 75 and 55 Ma). As such, there exist multiple locations where targeted drilling could recover depth or latitude transects of early Paleogene deep-sea sediment, and from which detailed carbonate accumulation records might be generated.

Cores examined in this study suggest that high-quality early Paleogene CCD records might be generated in the central Indian Ocean. Certainly, relatively thick lower Paleogene sediment sections exist, and microfossil assemblage, carbonate content and $\delta^{13}C$ variations within these sequences can be correlated to other locations. Missing are sites with multiple drill holes where sediment recovery occurs through advanced piston coring (APC) techniques.

In the last 15 years or so, two drilling strategies have been employed in the Atlantic and Pacific oceans to reconstruct early Paleogene oceanographic conditions, including carbonate saturation horizons (Zachos et al., 2004; Pälike et al., 2010). The "Walvis Ridge strategy" drills a series of sites down the flank of an aseismic ridge to obtain a depth transect (e.g., Zachos et al., 2004). This might be done on Ninetyeast Ridge, although ideally several hundred kilometers north of Site 214. The flanks of Ninetyeast Ridge in the vicinity of Site 214 have very little sediment (Veevers, 1974). By contrast, Site 216, also on the crest of Ninetyeast Ridge but 1550 km to the north, has a 457 m thick sediment section that terminates into Maastrictian basalt (Shipboard Scientific Party, 1974); the flanks of the ridge in this location also have moderately thick sediment sections (Veevers, 1974). (We note that sediment recovery was particularly poor at Site 216, so we omitted this location from our study and Fig. 11).

CPD
10, 3163–3221, 2014

The "Pacific Equatorial Age Transect" (PEAT) strategy drills multiple locations at a nominally fixed position perpendicular to a ridge axis (Pälike et al., 2010). With this approach, specific short time slices can be recovered along ancient ridge flanks. Transects could be drilled parallel to Ninetyeast Ridge, which might include re-drilling of Sites 213 and 215, as well as targeting sediment sequences to the north, which should hold variably thick carbonate intervals above tholeiitic basalt emplaced during the late Cretaceous and Paleocene.

6 Summary and conclusions

The early Paleogene was characterized by major changes in global carbon cycling as attested to by large amplitude variations in δ^{13}C records of carbonate and organic carbon. A full understanding of these changes necessitates detailed records of contemporaneous carbonate accumulation on the seafloor. Prior to our work, the early Paleogene CCD was poorly constrained, especially for the Indian Ocean. Moreover, δ^{13}C records and carbonate accumulation records rarely have been coupled together over Myr time intervals. We have revised the stratigraphy and generated new carbonate content and δ^{13}C records at three sites in the central Indian Ocean – Sites 213, 214, and 215, in an effort to fill these gaps.

Following our work and after considerable hindsight, we begin our conclusions with an admission: a detailed early Paleogene CCD curve for the central Indian Ocean, while crucial to understanding carbon cycling during this time (Zeebe et al., 2009; Cui et al., 2011; Komar et al., 2013), cannot be generated with sedimentary records at available drill sites. This problem arises from several basic problems, as highlighted by the chosen sites.

First, the tectonic history of the central Indian Ocean is complex and poorly constrained (Fisher and Sclater, 1983; Cande et al., 2010; Chatterjee et al., 2013). Reasonable estimates for initial depths and time trajectories can be derived for sites in the eastern Equatorial Pacific (Leon-Rodriguez and Dickens, 2010), the region from which

CPD
10, 3163–3221, 2014

the most detailed early Paleogene CCD records have emerged (Pälike et al., 2012). This luxury is not so clear for Sites 213, 214 and 215.

Second, the three sites contain fairly thick sediment sections that overlie Paleocene basalt in the central Indian Ocean. The material at these sites is suitable for generating detailed carbonate accumulation and $\delta^{13}C$ records. Although Site 214 is too shallow in the early Paleogene to provide constraints on carbon saturation horizons, Sites 213 and 215 appear ideally located during this time. However, only one hole was drilled at each site, and sediment coring occurred through rotary methods. Consequently, the recovered sections are incomplete and contain intervals with major sediment disturbance.

Third, new sites are required to fully address the problem. Even if Sites 213 and 215 were re-drilled with modern techniques, including APC, companion sites would have to be drilled to the north, where crustal ages are older. This is because the CCD likely shoaled in the middle to late Paleocene, and deepened in the late Paleocene to early Eocene.

Despite the above problems, the new records of carbonate content and $\delta^{13}C$ generated at Sites 213 and 215 add to our understanding of early Paleogene carbon cycling. The highs and lows in carbonate content and $\delta^{13}C$ appear related, and thus support ideas that major changes in net fluxes of organic carbon to and from the exogenic carbon cycle occurred during the early Paleogene.

The Supplement related to this article is available online at doi:10.5194/cpd-10-3163-2014-supplement.

Acknowledgements. This study used samples and data provided by the International Ocean Discovery Program. We thank workers from the Kochi Core Repository in Nankoku, Kochi, Japan for all the time they put into sampling DSDP Leg 22 Sites on our behalf. We thank G. Snyder for overseeing and managing sample preparation in the geochemistry laboratory at Rice University, and A. van Dijk for helping with stable isotope analyses at Utrecht University.

CPD
10, 3163–3221, 2014

Funding for this work principally came from NSF-FESD-OCE-1338842 awarded to C. T. Lee, G. R. Dickens and colleagues, and a Vici grant of the Netherlands Organisation for Scientific Research (NWO) awarded to L. J. Lourens. A. Sluijs thanks the European Research Council for ERC starting grant #259627 and the Royal Netherlands Academy of Arts and Sciences for a visiting professors grant for G. R. Dickens.

References

Agnini, C., Muttoni, G., Kent, D. V., and Rio, D.: Eocene biostratigraphy and magnetic stratigraphy from Possagno, Italy: the calcareous nannofossil response to climate variability, Earth Planet. Sc. Lett., 241, 815–830, 2006.

Agnini, C., Fornaciari, E., Raffi, I., Rio, D., Rohl, U., and Westerhold, T.: High-resolution nannofossil biochronology of middle Paleocene to early Eocene at ODP Site 1262: Implications for Calcareous nannoplankton evolution, Mar. Micropaleontol., 64, 215–248, 2007.

Berger, W. H.: Deep sea carbonates: dissolution facies and age-Depth constancy, Nature, 236, 392–395, 1972.

Berger, W. H.: Cenozoic sedimentation in the eastern tropical Pacific, Geol. Soc. Am. Bull., 84, 1941–1954, 1973.

Berggren, W. A. and Norris, R. D.: Biostratigraphy, Phylogeny, and Systematics of Paleocene Trochospiral Planktic Foraminifera, Micropaleontology Press, American Museum of Natural History, New York, NY, i-ii, 1–116, 1997.

Berggren, W. A. and Pearson, P. N.: A revised tropical Paleogene planktonic foraminiferal zonation, J. Foramin. Res., 35, 279–298, 2005.

Boudreau, B. P., Middelburg, J. J., and Meysman, F. J. R.: Carbonate compensation dynamics, Geophys. Res. Lett., 37, L03603, doi:10.1029/2009GL041847, 2010.

Broecker, W. S.: A need to improve reconstructions of the fluctuations in the calcite compensation depth over the course of the Cenozoic, Paleoceanography, 23, PAI204, doi:10.1029/2007PA001456, 2008.

Broecker, W. S. and Peng, T.-H.: Tracers in the Sea, Eldigio, Palisades, NY, 1–690, 1982.

Bukry, D.: Coccolith and silicoflagellate stratigraphy, Eastern Indian Ocean, Deep Sea Drilling Project, Leg 22, in: Initial Reports DSDP Leg 22, edited by: von der Borch, C. C. and Sclater, J. G., US Government Printing Office, Washington, 601–607, 1974.

CPD
10, 3163–3221, 2014

Calcagno, P. and Cazenave, A.: Subsidence of the seafloor in the Atlantic and Pacific Oceans: regional and large-scale variations, Earth Planet. Sc. Lett., 126, 473–492, 1994.
Cande, S. C., Patriat, P., and Dyment, J.: Motion between the Indian, Antarctic, and African plates in the early Cenozoic, Geophys. J. Int., 183, 127–149, 2010.
Carpenter, R. J., Truswell, E. M., and Harris, W. K.: Lauraceae fossils from a volcanic Palaeocene oceanic island, Ninetyeast Ridge, Indian Ocean: ancient long-distance dispersal?, J. Biogeogr., 37, 1202–1213, 2010.
Charles, A. J., Condon, D. J., Harding, I. C., Pälike, H., Marshall, J. E. A., Cui, Y., Kump, L., and Croudace, I. W.: Constraints on the numerical age of the Paleocene-Eocene boundary, Geochem. Geophy. Geosy., 12, Q0AA17, doi:10.1029/2010GC003426, 2011.
Chatterjee, S., Goswami, A., and Scotese, C. R.: The longest voyage: tectonic, magmatic, and paleoclimatic evolution of the Indian plate during its northward flight from Gondwana to Asia, Gondwana Res., 23, 238–267, 2013.
Cochran, J. R.: Variations in subsidence rates along intermediate and fast spreading mid-ocean ridges, Geophys. J. Roy. Astr. S., 87, 421–454, 1986.
Coplen, T. B., Brand, W. A., Gehre, M., Gröning, M., Meijer, H. A. J., Toman, B., and Verkouteren, M.: New guidelines for δ^{13}C measurements, Anal. Chem., 78, 2439–2441, 2006.
Cramer, B. S., Wright, J. D., Kent, D. V., and Aubry, M.-P.: Orbital climate forcing of δ^{13}C excursion in the late Paleocene-early Eocene (chrons C24n-C25n), Paleoceanography, 18, 1097, doi:10.1029/2003PA000909, 2003.
Cui, Y., Kump, L. R., Ridgwell, A. J., Charles, A. J., Junium, C. K., Diefendorf, A. F., Freeman, K. H., Urban, N. M., and Harding, I. C.: Slow release of fossil carbon during the Palaeocene-Eocene thermal maximum, Nat. Geosci., 4, 481–485, 2011.
Detrick, R. S., Sclater, J. G., and Thiede, J.: The subsidence of aseismic ridges, Earth Planet. Sc. Lett., 34, 185–196, 1977.
Dickens, G. R.: Rethinking the global carbon cycle with a large, dynamic and microbially mediated gas hydrate capacitor, Earth Planet. Sc. Lett., 213, 169–183, 2003.
Dickens, G. R.: Down the Rabbit Hole: toward appropriate discussion of methane release from gas hydrate systems during the Paleocene-Eocene thermal maximum and other past hyperthermal events, Clim. Past, 7, 831–846, doi:10.5194/cp-7-831-2011, 2011.
Dickens, G. R. and Backman, J.: Core alignment and composite depth scale for the lower Paleogene through uppermost cretaceous interval at deep sea drilling project site 577, Newsl. Stratigr., 46, 47–68, 2013.

CPD
10, 3163–3221, 2014

Dickens, G. R., Castillo, M. M., and Walker, J. C. G.: A blast of gas in the latest Paleocene: simulating first-order effects of massive dissociation of oceanic methane hydrate, Geology, 25, 259–262, 1997.

Dickens, G. R., O'Neil, J. R., Rea, D. K., and Owen, R. M.: Dissociation of oceanica methane hydrate as a cause of the carbon isotope excursion at the end of the Paleocene, Paleoceanography, 10, 965–971, 1995.

Expedition 329 Scientists: Site U1370, in: Proc. of the IODP, vol. 329, edited by: D'Hondt, S., Inagaki, F., Alvarez Zarikian, C. A., and the Expedition 329 Scientists, Integrated Ocean Drilling Program Management International Inc., Tokyo, 1–81, doi:10.2204/iodp.proc.329.108.2011, 2011.

Fisher, R. L. and Sclater, J. G.: Tectonic evolution of the Southwest Indian Ocean since the Mid-Cretaceous: plate motions and stability of the pole of Antarctica/Africa for at least 80 Myr, Geophys. J. Roy. Astr. S., 73, 553–576, 1983.

Frey, F. A., Dickey Jr., J. S., Thompson, G., and Bryan, W. B.: Eastern Indian Ocean DSDP sites: correlations between petrography, geochemistry and tectonic setting, in: A Synthesis of Deep Sea Drilling in the Indian Ocean, edited by: Heirtzler, J. R., and Sclater, J. G., US Government Printing Office, Washington DC, 189–257, 1977.

Frey, F. A., Jones, W. B., Davies, H., and Weis, D.: Geochemical and petrologic data for basalts from Site 756, 757, and 758: implications for the origin and evolution of Ninetyeast Ridge, in: Proc. ODP Sci. Results, vol. 121, edited by: Weissel, J., Peirce, J., Taylor, E., Alt, J., et al., Ocean Drilling Program, College Station, TX , 611–659, 1991.

Frey, F. A., Pringle, M., Meleney, P., Huang, S., and Piotrowski, A.: Diverse mantle sources for Ninetyeast Ridge magmatism: geochemical constraints from basaltic glasses, Earth Planet. Sc. Lett., 303, 215–224, 2011.

Galeotti, S., Krishnan, S., Pagani, M., Lanci, L., Gaudio, A., Zachos, J. C., Monechi, S., Morelli, G., and Lourens, L.: Orbital chronology of early Eocene hyperthermals form the Contessa Road Section, central Italy, Earth Planet. Sc. Lett., 290, 192–200, 2010.

Gartner, S.: Nannofossil biostratigraphy, Leg 22. Deep Sea Drilling Project, in: Initial Reports, DSDP Leg 22, edited by: von der Borch, C. C. and Sclater, J. G., US Government Printing Office, Washington, 577–599, doi:10.2973/dsdp.proc.22.126.1974, 1974.

Hagelberg, T., Shackleton, N., Pisias, N., and Shipboard Scientific Party: Development of composite depth sections for Sites 844 through 854, in: Proceedings of the Ocean Drilling Pro-

CPD
10, 3163–3221, 2014

gram, Initial Reports, vol. 138, edited by: Mayer, L., Pisias, N., Janecek, T. et al., Ocean Drilling Program, College Station, TX, 79–85, 1992.
Hancock, H. J. L., Dickens, G. R., Thomas, E., and Blake, K. L.: Reappraisal of early Paleogene CCD curves: foraminiferal assemblages and stable carbon isotopes across the carbonate facies of Perth Abyssal Plain, Int. J. Earth Sci., 96, 925–946, 2007.
Hilgen, F. J., Kuiper, K. F., and Lourens, L. J.: Evaluation of the astronomical time scale for the Paleocene and earliest Eocene, Earth Planet. Sc. Lett., 300, 139–151, 2010.
Hovan, S. A. and Rea, D. K.: Paleocene/Eocene boundary changes in atmospheric and oceanic circulation: a Southern Hemisphere record, Geology, 20, 15–18, 1992.
Kelly, D. C., Nielsen, T. M. J., McCarren, H. K., Zachos, J. C., and Röhl, U.: Spatiotemporal patterns of carbonate sedimentation in the South Atlantic: implications for carbon cycling during the Paleocene–Eocene thermal maximum, Palaeogeogr. Palaeocl., 293, 30–40, 2010.
Kelly, D. C., Nielsen, T. M. J., and Schellenberg. S. A.: Carbonate saturation dynamics during the Paleocene-Eocene thermal maximum: bathyal constraints from ODP sites 689 and 690 in the Weddell Sea (South Atlantic), Mar. Geol., 303–306, 75–86, 2012.
Kennett, J. P.: Marine Geology, Prentice-Hall, Inc., Englewood Cliffs, NJ, 1–813, 1982.
Kennett, J. P. and Stott, L. D.: Abrupt deep-sea warming, palaeoceanographic changes and benthic extinctions at the end of the Palaeocene, Nature, 353, 225–229, 1991.
Klein, E. M., Langmuir, C. H., and Staudigel, H.: Geochemistry of basalts from the southeast Indian Ridge, 115–138° E, J. Geophys. Res., 96, 2089–2107, 1991.
Komar, N., Zeebe, R. E., and Dickens, G. R.: Understanding long-term carbon cycle trends: the late Paleocene through the early Eocene, Paleoceanography, 28, 650–662, 2013.
Kump, L. R., Bralower, T. J., and Ridgwell, A.: Ocean acidification in deep time, Oceanography, 22, 94–107, 2009.
Kurtz, A. C., Kump, L. R., Arthur, M. A., Zachos, J. C., and Paytan, A.: Early Cenozoic decoupling of the global carbon and sulfur cycles, Paleoceanography, 18, 1090, doi:10.1029/2003PA000908, 2003.
Leon-Rodriguez, L. and Dickens, G. R.: Constraints on ocean acidification associated with rapid and massive carbon injections: the early Paleogene record at ocean drilling program site 1215, equatorial Pacific Ocean, Palaeogeogr. Palaeocl., 298, 409–420, 2010.
MacDougall, J. D.: Uranium in marine basalts: concentration, distribution and implications, Earth Planet. Sc. Lett., 35, 65–70, 1977.

CPD
10, 3163–3221, 2014

Mahoney, J. J., Graham, D. W., Christie, D. M., Johnson, K. T. M., Hall, L. S., and Vonderhaar, D. L.: Between a hotspot and a cold spot: isotopic variation in the Southeast Indian Ridge Asthenosphere, 86–118° E, Journal of Petrology, 43, 1155–1176, 2002.
Martini, E.: Standard tertiary and quaternary calcareous nannoplankton zonation, in: Proceedings of the 2nd International Conference of Planktonic Microfossils Roma, edited by: Farinacci, A., Rome (Ed. Tecnosci.), 2, 739–785, 1971.
McGowran, B.: Foraminifera, Leg 22. Deep Sea Drilling Project, in: Initial Reports, DSDP Leg 22, edited by: von der Borch, C. C., and Sclater, J. G., US Government Printing Office, Washington, 577–599, 1974.
McKenzie, D. and Sclater, J. G.: The evolution of the Indian Ocean since the Late Cretaceous, Geophys. J. Roy. Astr. S., 25, 437–528, 1971.
Nicolo, M. J., Dickens, G. R., Hollis, C. J., and Zachos, J. C.: Multiple early Eocene hyperthermals: their sedimentary expression on the New Zealand continental margin and in the deep sea, Geology, 35, 699–702; doi:10.1130/G23648A.1, 2007.
Ocean Drilling Stratigraphic Network: available at: http://www.odsn.de, 2011.
Pälike, H., Nishi, H., Lyle, M., Raffi, I., Gamage, K., Klaus, A., and the Expedition 320/321 Scientists: Expedition 320/321 summary, in: Proceedings of the Integrated Ocean Drilling Program, 320/321, edited by: Pälike, H., Lyle, M., Nishi, H., Raffi, I., Gamage, K., Klaus, A., and the Expedition 320/321 Scientists, Integrated Ocean Drilling Program Management International, Inc., Tokyo, doi:10.2204/iodp.proc.320321.101.2010, 2010.
Pälike, H., Lyle, M. W., Nishi, H. et al.: A Cenozoic record of the equatorial Pacific carbonate compensation depth, Nature, 488, 609–615, 2012.
Parsons, B. and Sclater, J. G.: An analysis of the variation of ocean floor bathymetry and heat flow with age, J. Geophys. Res., 82, 803–827, 1977.
Patriat, P. and Achache, J.: India-Eurasia collision chronology has implications for crustal shortening and driving mechanisms of plates, Nature, 311, 615–621, 1984.
Patterson, W. P. and Walter, L. M.: Syndepositional diagenesis of modern platform carbonates: evidence from isotopic and minor element data, Geology, 22, 127–130, 1994a.
Patterson, W. P. and Walter, L. M.: Depletion of 13C in seawater ΣCO_2 on modern carbonate platforms: significance for the carbon isotopic record of carbonates, Geology, 22, 885–888, 1994b.
Peirce, J. W.: The northward motion of India since the Late Cretaceous, Geophys. J. R. Astr. Soc., 52, 277–311, 1978.

CPD
10, 3163–3221, 2014

Pimm, A. C.: Sedimentology and History of the Northeastern Indian Ocean from late Cretaceous to recent, in: Initial Reports of the Deep Sea Drilling Project, vol. 22, edited by: von der Borch, C. C., Sclater, J. G., et al., US Government Printing Office, Washington, 717–803, 1974.

Ravizza, G., Norris, R. N., Blusztajn, J., and Aubry, M- P.: An osmium isotope excursion associated with the late Paleocene thermal maximum: evidence of intensified chemical weathering, Paleoceanography, 16, 155–163, doi:10.1029/2000PA000541, 2001.

Rea, D. K. and Lyle, M. W.: Paleogene calcite compensation depth in the eastern subtropical Pacific: answers and questions, Paleoceanography, 20, PA1012, doi:10.1029/2004PA001064, 2005.

Ruddiman, W. F., Cameron, D., and Clement, B. M.: Sediment disturbance and correlation of offset holds drilled with the hydraulic piston corer, Leg 94, in: Initial Reports of the Deep Sea Drilling Project Leg 94, edited by: Ruddiman, W. F., Kidd, R. B., Thomas, E. et al., 1987, US Government Printing Office, Washington, 1987.

Sanders, D.: Syndepositional dissolution of calcium carbonate in neritic carbonate environments: geological recognition, processes, potential significance, J. Afr. Earth Sci., 36, 99–134, 2003.

Saunders, A. D., Storey, M., Gibson, I. L., Leat, P., Hergt, J., and Thompson, R. N.: Chemical and Isotopic Constraints on the origin of basalts from Ninetyeast Ridge, Indian Ocean: results from DSDP Legs 22 and 26 and ODP Leg 121, in: Proceedings of the Ocean Drilling Program, Scientific Results, vol. 121, edited by: Weissel, J., Peirce, J., Taylor, E., Alt, J. et al., Ocean Drilling Program, College Station, TX, 559–590, 1991.

Sclater, J. G., Anderson, R. N., and Lee Bell, M.: Elevation of ridges and evolution of the Central Eastern Pacific, J. Geophys. Res., 76, 7888–7915, 1971.

Shackleton, N. J.: Paleogene Stable Isotope Events, Palaeogeogr. Palaeocl., 57, 91–102, 1986.

Shackleton, N. J., Hall, M. A., and Bleil, U.: Carbon-isotope stratigraphy, site 577, in: Initial Reports of the Deep Sea Drilling Project, vol. 86, edited by: Turner, K. L., US Government Printing Office, Washington, 503–511, 1985.

Shipboard Scientific Party: Site 216, in: Initial Reports of the Deep Sea Drilling Project, vol. 22, edited by: von der Borch, C. C., Sclater, J. G., et al., US Government Printing Office, Washington, 213–265, 1974a.

CPD
10, 3163–3221, 2014

Shipboard Scientific Party: Site 236, in: Initial Reports of the Deep Sea Drilling Project, vol. 24, edited by: Fisher, R. L., Bunce, E. T., et al., U S. Government Printing Office, Washington, 327–389, 1974b.
Shipboard Scientific Party: Site 245, in: Initial Reports of the Deep Sea Drilling Project, Volume 25, edited by: Simpson, E. S. W., Schlich, R., et al., US Government Printing Office, Washington, 187–236, 1974c.
Shipboard Scientific Party: Site 756, in: ODP Init. Reps, 121, edited by: Peirce, J., Weissel, J. et al., Ocean Drilling Program, College Station, TX, 259–303, 1989a.
Shipboard Scientific Party: Site 757, in: Proc. ODP Init. Reps, 121, edited by: Peirce, J., Weissel, J. et al., Ocean Drilling Program, College Station, TX, 305–358, 1989b.
Shipboard Scientific Party: Site 758, in: Proc. ODP Init. Reps, 121, edited by: Peirce, J., Weissel, J. et al., College Station, TX, Ocean Drilling Program, 359–453, 1989c.
Shipboard Scientific Party: Site 766, in: Proc. ODP Init. Reps, 123, edited by: Gradstein, F. M., Ludden, J. N., Adamson, A. C. et al., Ocean Drilling Program, College Station, TX, 269–352, 1990.
Shipboard Scientific Party: Leg 179 summary, in: Proc. ODP, Init. Reps., 179, edited by: Pettigrew, T. L., Casey, J. F., Miller, D. J. et al., Ocean Drilling Program, College Station, TX, 1–26, 1999.
Shipboard Scientific Party: Site 1219, in: Proc. ODP Init. Reps, 199, edited by: Lyle, M., Wilson, P. A., Janecek, T. R. et al., Ocean Drilling Program, College Station, TX, 1–129, 2002a.
Shipboard Scientific Party: Site 1220, in: Proc. ODP Init. Reps, 199, edited by: Lyle, M., Wilson, P. A., Janecek, T. R. et al., Ocean Drilling Program, College Station, TX, 1–93, 2002b.
Slotnick, B. S., Dickens, G. R., Nicolo, M. J., Hollis, C. J., Crampton, J. S., and Zachos, J. C., Sluijs, A.: Numerous large amplitude variations in carbon cycling and terrestrial weathering throughout the latest Paleocene and earliest Eocene, J. Geol., 120, 487–505, 2012.
Sluijs, A., Bowen, G., Brinkhuis, H., Lourens, L. J., and Thomas, E.: The Palaeocene-Eocene Thermal Maximum super greenhouse: biotic and geochemical signatures, age models and mechanisms of global change, in: Deep-Time Perspectives on Climate Change: Marrying the Signal from Computer Models and Biological Proxies, edited by: Williams, M., Haywood, A. M., Gregory, J., and Schmidt, D. N., The Micropaleontological Society, Special Publications, London, 323–349, 2007.

CPD
10, 3163–3221, 2014

Stap, L., Sluijs, A., Thomas, E., and Lourens, L.: Patterns and magnitude of deep sea carbonate dissolution during Eocene Thermal Maximum 2 and H2, Walvis Ridge, southeastern Atlantic Ocean, Paleoceanography, 24, PA1211, doi:10.1029/2008PA001655, 2009.

Stap, L., Lourens, L. J., Thomas, E., Sluijs, A., Bohaty, S., and Zachos, J. C.: High resolution deep-sea carbon and oxygen isotope records of Eocene thermal maximum 2 and H2, Geology, 38, 607–610, 2010.

Storms, M. A.: Ocean Drilling Program (ODP) Deep Sea Coring Techniques, Mar. Geophys. Res., 12, 109–130, 1990.

Swart, P. K. and Eberli, G.: The nature of the $\delta^{13}C$ of periplatform sediments: implications for stratigraphy and the global carbon cycle, Sediment. Geol., 175, 115–129, 2005.

Tremolada, R. and Bralower, T. J.: Nannofossil assemblage fluctuations during the Paleocene–Eocene Thermal Maximum at Sites 213 (Indian Ocean) and 401 (North Atlantic Ocean): palaeoceanographic implications, Mar. Micropaleontol., 52, 107–116, 2004.

van Andel, T. H.: Mesozoic/Cenozoic Calcite Compensation Depth and the global distribution of calcareous sediments, Earth Planet. Sc. Lett., 26, 187–194, 1975.

Vandenberghe, N., Hilgen, F. J., Speijer, R. P.: The Paleogene period, in: The Geologic Time Scale 2012, edited by: Gradstein, F., Ogg, J., Schmitz, M., Ogg, G., Elsevier BV, Amsterdam, the Netherlands, 855–922, 2012.

Veevers, J. J.: 10. Seismic profiles made underway on Leg 22, in: Initial Reports, DSDP Leg 22, edited by: von der Borch, C. C., and Sclater, J. G., US Government Printing Office, Washington, 351–367, 1974.

von der Borch, C. C. and Sclater, J. G.: Initial Reports, DSDP Leg 22, US Government Printing Office Washington, 1–599, doi:10.2973/dsdp.proc.22.126.1974, 1974.

Westerhold, T. and Röhl, U.: High resolution cyclostratigraphy of the early Eocene – new insights into the origin of the Cenozoic cooling trend, Clim. Past, 5, 309–327, doi:10.5194/cp-5-309-2009, 2009.

Westerhold, T., Röhl, U., Raffi, I., Fornaciari, E., Monechi, S., Reale, V., Bowles, J., and Evans, H. F.: Astronomical calibration of the Paleocene time, Palaeogeogr. Palaeocl., 257, 377–403, 2008.

Zachos, J. C., Rea, D. K., Seto, K., Nomura, R., and Niitsuma, N.: Paleogene and early Neogene deep water paleoceanography of the Indian Ocean as determined from Benthic foraminifer stable carbon and oxygen isotope records, Geoph. Monog. Series, 70, 351–385, 1992.

CPD
10, 3163–3221, 2014

Zachos, J. C., Pagani, M., Sloan, L., Thomas, E., and Billups, K.: Trends, rhythms, and aberrations in global climate 65 Ma to present, Science, 292, 686–693, doi:10.1126/science.1059412, 2001.

Zachos, J. C., Kroon, D., Blum, P., Bowles, J., Gaillot, P., Hasegawa, T., Hathorne, E. C., Hodell, D. A., Kelly, D. C., Jung, J.-H., Keller, S. M., Lee, Y. S., Leuschner, D. C., Liu, Z., Lohmann, K. C., Lourens, L., Monechi, S., Nicolo, M., Raffi, I., Riesselman, C., Röhl, U., Schellenberg, S. A., Schmidt, D., Sluijs, A., Thomas, D., Thomas, E., and Vallius, H.: Proceedings of the Ocean Drilling Program, Initial Reports, vol. 208, doi:10.2973/odp.proc.ir.208.2004, 2004.

Zachos, J. C., Röhl, U., Schellenberg, S. A., Sluijs, A., Hodell, D. A., Kelly, D. C., Thomas, E., Nicolo, M., Raffi, I., Lourens, L. J., McCarren, H., and Kroon, D.: Rapid acidification of the Ocean during the Paleocene–Eocene thermal maximum, Science, 208, 1611–1615, 2005.

Zachos, J. C., McCarren, H., Murphy, B., Rohl, U., and Westerhold, T.: Tempo and scale of late Paleocene and early Eocene carbon isotope cycles: implications for the origin of hyperthermals, Earth Planet. Sc. Lett., 299, 242–249, doi:10.1016/j.epsl.2010.09.004, 2010.

Zeebe, R. E. and Westbroek, P.: A simple model for the $CaCO_3$ saturation state of the ocean: the "Strangelove," the "Neritan," and the "Cretan" Ocean, Geochem. Geophy. Geosy., 4, 1104, doi:10.1029/2003GC000538, 2003.

Zeebe, R. E., Zachos, J. C., and Dickens, G. R.: Carbon dioxide forcing along insufficient to explain Palaeocene–Eocene thermal maximum warming, Nat. Geosci., 2, 576–580, doi:10.1038/NGEO578, 2009.

CPD
10, 3163–3221, 2014

Table 1. Paleomagnetic and nannofossil age estimates for the Paleocene and early Eocene.

	Age Datum		W-O1 Age [1] (Ma)	GPTS 2004 Age [2] (Ma)	Zone Base
N	Base	*Discoaster sublodoensis*	49.5		NP14
N	Top	*Tribrachiatus orthostylus*	50.7		
E	Base	K/X hyperthermal	52.50		
N	Base	*Discoaster lodoensis*	53.24	53.11	NP12
N	Top	*Discoaster multiradiatus*	53.24	53.11	
E	Base	ETM2/H1 hyperthermal	53.73		
N	Top	*Tribrachiatus contortus*	53.80	53.49	
N	Base	*Sphenolithus radians*	53.85	53.53	
N	Base	*Tribrachiatus orthostylus*	54.00	53.67	NP11
N	Base	*Tribrachiatus contortus*	54.34	54.00	
N	Base	*Discoaster diastypus*	54.48	54.13	NP10
N	Top	*Fasciculithus* spp.	55.11	54.71	
N		*Fasciculithus decrease*	55.47		
N	Crossover	*Zygrhablithus bijugatus/Fasciculithus tympaniformis*	55.47		
E	Base	PETM hyperthermal	55.53	55.00	
N	Top	*Ericsonia robusta*	56.66		
N	Base common	*Discoaster multiradiatus*	56.76	56.01	NP9
N	Top	*Discoaster okadai*	56.85	56.12	
N	Base	*Discoaster okadai*	56.95	56.23	
N	Base	*Discoaster nobilis*	56.97	56.25	
N	Base	*Ericsonia robusta*	57.04		
N	Top	*Heliolithus kleinpellii*	58.33	57.42	
N	Base	*Discoaster mohleri*	58.55	57.57	NP7
N	Top	*Heliolithus cantabriae*	58.64		
N	Base	*Heliolithus kleinpellii*	59.02	58.03	NP6
N	Base	*Heliolithus cantabriae*	59.37		
N	Base	Fasciculithus tympaniformis	60.9		
N	Base	*Fasciculithus* spp.	61.21	60.31	NP5*
N	Base	*Sphenolithus* spp.	61.59	60.74	

Notes:
[1] Ages to the nearest 0.1 Ma as reported by Agnini et al. (2007) and Westerhold et al. (2008); W-O1 = Westerhold Option 1; N = Nannofossil datum; E = Carbon Isotope Excursion datum.
[2] GPTS 2004. Ages slightly differ between papers (e.g. Agnini et al., 2007 and Westerhold et al., 2008)
* The actual NP5 start is for F. tympanformis at ca. 60.9 Ma.

CPD
10, 3163–3221, 2014

Table 2. Site 213.

Core	Section	cm ±1	mbsf	mcd	Type	Nannofossil indicators	Abundance	Preservation	Min. Age (Ma)	Max. Age (Ma)	Zone
14	5	25	129.25	130.24	Presence/Presence	*Tribrachiatus orthostylus/Discoaster lodoensis*	F	P	50.70	53.24	NP12
14	5	65	129.65	130.64	Presence/Presence	*Tribrachiatus orthostylus/Discoaster lodoensis*	F	P	50.70	53.24	NP12
14	5	85	129.85	130.84	Presence/Presence	*Tribrachiatus orthostylus/Discoaster lodoensis*	F	P	50.70	53.24	NP12
14	6	69	131.19	132.18	Presence/Presence	*Tribrachiatus orthostylus/Discoaster lodoensis*	C	P	50.70	53.24	NP12
15	1	20.5	132.71	134.70		*barren*					NP12
15	1	101	133.51	135.50		*barren*					NP12
15	2	31	134.31	136.30	Presence/Presence	*Tribrachiatus orthostylus/Discoaster lodoensis*	C	P	50.70	53.24	NP12
15	2	71	134.71	136.70	Presence/Presence	*Tribrachiatus orthostylus/Discoaster lodoensis*	C	P	50.70	53.24	NP12
15	3	3	135.53	137.52	Presence/Presence	*Tribrachiatus orthostylus/Discoaster lodoensis*	C	P	50.70	53.24	NP12
15	3	41	135.91	137.90	Presence/Presence	*Tribrachiatus orthostylus/Discoaster lodoensis* (rare)	A	P	50.70	53.24	NP12
15	3	121	136.71	138.70	Presence/Presence	*Tribrachiatus orthostylus/Discoaster lodoensis* (rare)	A	P	50.70	53.24	NP12
15	4	31	137.32	139.31	Absence/Presence	*Discoaster lodoensis/Sphenolithus radians*	A	P	53.24	53.85	NP11
15	4	101.5	138.015	140.01	Absence/Presence	*Discoaster lodoensis/Sphenolithus radians*	A	P	53.24	53.85	NP11
15	5	121	139.71	141.70	Absence/Presence	*Tribrachiatus orthostylus/Discoaster diastypus*	A	P/M	54.00	54.48	NP10
15	6	54	140.54	142.53	Absence/Presence	*Tribrachiatus orthostylus/Discoaster diastypus*	A	P/M	54.00	54.48	NP10
16	1	83	142.83	145.82	Presence/Presence	*Fasciculithus tympaniformis* (few)/*Zygrhablithus bijugatus*	A	M	55.11	55.47	NP9
16	2	140	144.33	147.89	Presence/Presence	*Fasciculithus tympaniformis* (few)/*Zygrhablithus bijugatus*	A	M	55.11	55.47	NP9
16	3	68	145.68	148.67	Presence/Presence	*Fasciculithus tympaniformis* (few)/*Zygrhablithus bijugatus*	A	M	55.11	55.47	NP9

CPD
10, 3163–3221, 2014

Table 3. Site 214.

Core	Section	cm ±1	mbsf	mcd	Type	Nannofossil indicators	Abundance	Preservation	Min. Age (Ma)	Max. Age (Ma)	Zone
34	1	51	314.51	314.95	Presence	*Tribrachiatus orthostylus/Discoaster lodoensis*	A	P	50.70	53.24	NP12
34	2	101	316.51	316.95	Presence	*Tribrachiatus orthostylus/Discoaster lodoensis*	A	P	50.70	53.24	NP12
34	3	111	318.11	318.55	Presence	*Tribrachiatus orthostylus/Discoaster lodoensis*	A	P	50.70	53.24	NP12
34	4	41	318.91	319.35	Presence	*Tribrachiatus orthostylus/Discoaster lodoensis*	A	P	50.70	53.24	NP12
34	6	134.5	322.845	323.285	Presence	*Tribrachiatus orthostylus/Discoaster lodoensis*	A	P	50.70	53.24	NP12
35	1	16.5	323.665	324.65	Presence	*Tribrachiatus orthostylus/Discoaster lodoensis*	A	P	50.70	53.24	NP12
35	2	3	325.03	326.02	Presence	*Tribrachiatus orthostylus/Discoaster lodoensis*	C	P	50.70	53.24	NP12
35	3	39	326.89	327.88	Presence	*Tribrachiatus orthostylus/Discoaster lodoensis*	C	P	50.70	53.24	NP12
35	4	141	328.41	330.4	Absence/Presence	*Discoaster lodoensis/Sphenolithus radians*	C	P	53.24	53.85	NP11
36	2	121	335.71	337.7	Presence	*Heliolithus kleinpellii*	F	P	58.33	59.02	NP6
36	3	129	337.29	339.28	Presence	*Heliolithus kleinpellii*	C	M	58.33	59.02	NP6
36	4	61	338.11	340.1	Presence	*Heliolithus kleinpellii*	C	M	58.33	59.02	NP6
37	1	51	343.01	346.02	Absence/Presence	*Helilithus kleinpellii/Heliolithus cantabriae*	F	P	59.02	59.25	NP5
38	1	111	353.11	357.09	Absence/Presence	*Heliolithus cantabriae/Fasciculithus* spp.	F	P	59.25	60.85	NP5
38	2	81	354.31	358.3	Absence/Presence	*Heliolithus cantabriae/Fasciculithus* spp.	F	P	59.25	60.85	NP5
38	3	9.5	355.095	359.085	Absence/Presence	*Heliolithus cantabriae/Fasciulithus tympaniformis*	F	P	59.25	60.85	NP5
38	4	98.5	357.485	361.475	Presence	*Fasciculithus* spp.	F	P	59.25	61.21	NP4-5
39	1	114.5	362.645	367.635	Presence	*Fasciculithus* spp.	F	P	59.25	61.21	NP4-5
39	2	38.5	363.385	368.375	Presence	*Fasciculithus* spp.	F	P	59.25	61.21	NP4-5
39	3	51	365.01	370	Presence	*Fasciculithus* spp.	F	P	59.25	61.21	NP4-5

CPD
10, 3163–3221, 2014

Table 4. Site 215.

Core	Section	cm ±1	mbsf	mcd	Type	Nannofossil indicators	Abundance	Preservation	Min. Age (Ma)	Max. Age (Ma)	Zone
9	3	82	77.82	78.82	Presence	*Tribrachiatus orthostylus/Discoaster lodoensis*	F	P	50.7	53.24	NP12
9	3	106	78.06	79.05	Presence	*Tribrachiatus orthostylus/Discoaster lodoensis*	F	P	50.7	53.24	NP12
9	3	141	78.41	79.4	Presence	*Tribrachiatus orthostylus/Discoaster lodoensis*	F	P	50.7	53.24	NP12
10	1	141	84.91	86.9	Presence	*Tribrachiatus orthostylus/Discoaster lodoensis*	A	P	50.7	53.24	NP12
10	2	109	86.09	88.08	Absence/Presence	*Discoaster lodoensis/Sphenolithus radians*	A	P	53.24	53.85	NP11
10	3	[a]42.5	86.925	88.9	Absence/Presence	*Tribrachiatus orthostylus/Discoaster diastypus*	A	M	54	54.48	NP10
11	2	[a]80.5	95.305	98.3	Absence/Presence	*Tribrachiatus orthostylus/Discoaster diastypus*	A	M	54	54.48	NP10
11	4	20	97.7	100.69	Absence	*Discoaster diastypus/Fasciculithus tympaniformis*	A	M	54.48	55.11	NP9
11	5	111	100.11	103.1	Presence	*Fasciculithus tympaniformis* (few)/*Zygrhablithus bijugatus*	A	M	55.11	55.47	NP9
11	6	138.5	101.885	104.875	Presence	*Fasciculithus tympaniformis* (few)/*Zygrhablithus bijugatus*	A	M	55.11	55.47	NP9
12	2	141	105.41	109.4	Presence/Absence	Diverse*Fasciculithus* spp./*Ericsonia robusta*	A	M	55.53	56.64	NP9
12	3	21	105.71	109.7	Presence/Absence	Diverse*Fasciculithus* spp./*Ericsonia robusta*	A	M	55.53	56.64	NP9
12	5	142	109.92	113.91	Presence/Absence	Diverse*Fasciculithus* spp./*Ericsonia robusta*	A	M	55.53	56.64	NP9
12	6	141	111.41	115.4	Presence/Absence	Diverse*Fasciculithus* spp./*Ericsonia robusta*	A	M	55.53	56.64	NP9
13	2	3	113.53	118.53	Presence	*Ericsonia robusta/Discoaster multiradiatus*	A	M	56.64	56.76	NP9
13	3	43	115.43	120.43	Absence/Presence	*Discoaster multiradiatus/Ericsonia robusta*	A	M	56.76	56.86	NP7-8
13	4	104	117.54	122.54	Absence/Presence	*Discoaster multiradiatus/Ericsonia robusta*	A	M	56.76	56.86	NP7-8
14	1	15	121.65	127.64	Absence/Presence	*Discoaster multiradiatus/Ericsonia robusta*	A	M	56.76	56.86	NP7-8
14	2	103	124.03	130.02	Absence/Presence	*Ericsonia robusta/Discoster mohleri*	A	M	56.86	58.55	NP7-8
14	4	40.5	126.405	132.395	Absence/Presence	*Ericsonia robusta/Discoster mohleri*	A	M	56.86	58.55	NP7-8
14	5	11	127.61	133.6	Absence/Presence	*Ericsonia robusta/Discoster mohleri*	A	M	56.86	58.55	NP7-8
14	5	131	128.81	134.8	Absence/Presence	*Ericsonia robusta/Discoster mohleri*	A	M	56.86	58.55	NP7-8
14	6	101	130.01	136	Absence/Presence	*Ericsonia robusta/Discoster mohleri*	A	M	56.86	58.55	NP7-8

CPD
10, 3163–3221, 2014

Table 5. Site 213.

Core	Section	Top (cm)	Bottom (cm)	Mid (cm)	mbsf	mcd	$\delta^{13}C$	$\delta^{18}O$	$CaCO_3$ (%)	Source
13	1	30	32	31	113.80	113.80			1.12	this study
13	1	80	82	81	114.30	114.30			1.11	this study
13	1	130	132	131	114.80	114.80			1.28	this study
13	2	30	32	31	115.30	115.30			1.06	this study
13	2	80.5	82.5	81.5	115.81	115.81			1.03	this study
13	2	130	132	131	116.30	116.30			1.19	this study
13	3	30	32	31	116.80	116.80			1.06	this study
13	3	80	82	81	117.30	117.30			1.27	this study
13	3	130	132	131	117.80	117.80			1.09	this study
13	4	30	32	31	118.30	118.30			1.22	this study
13	4	80	82	81	118.80	118.80			1.13	this study
13	4	130.0	132	131	119.30	119.30			0.88	this study
13	5	30	32	31	119.80	119.80			0.93	this study
13	5	80	82	81	120.30	120.30			1.40	this study
13	5	130	132	131	120.80	120.80			0.82	this study
13	6	30	32	31	121.30	121.30			1.04	this study
13	6	80	82	81	121.80	121.80			1.00	this study
13	6	124.5	126.5	125.5	122.25	122.25			0.75	this study
14	1	20	22	21	123.20	124.20			1.10	this study
14	1	60	62	61	123.60	124.60			0.90	this study
14	1	100	102	101	124.00	125.00			1.77	this study
14	1	139.5	141.5	140.5	124.40	125.40			0.87	this study
14	2	30	32	31	124.80	125.80			0.65	this study
14	2	70	72	71	125.20	126.20			0.84	this study
14	2	110	112	111	125.60	126.60			0.90	this study
14	3	2	4	3	126.02	127.02			1.14	this study
14	3	40	42	41	126.40	127.40			0.82	this study
14	3	80	82	81	126.80	127.80			1.52	this study
14	3	120	122	121	127.20	128.20			0.74	this study
14	4	10	12	11	127.60	128.60			1.26	this study
14	4	50	52	51	128.00	129.00			0.75	this study
14	4	90	92	91	128.40	129.40			0.88	this study
14	4	130	132	131	128.80	129.80			0.73	this study
14	5	8	10	9	129.08	130.08	2.12	−1.20	18.73	this study
14	5	24	26	25	129.24	130.24	2.18	−1.93	21.45	this study
14	5	36	38	37	129.36	130.36	1.95	−1.60	29.20	this study
14	5	50	52	51	129.50	130.50	1.97	−1.60	39.83	this study
14	5	64	66	65	129.64	130.64	1.87	−1.73	44.30	this study
14	5	74	76	75	129.74	130.74	1.68	−1.40	16.90	this study
14	5	84	86	85	129.84	130.84	2.03	−1.73	35.95	this study
14	5	100	102	101	130.00	131.00	1.86	−1.59	30.44	this study
14	5	120	122	121	130.20	131.20	1.59	−1.28	24.72	this study
14	5	138	140	139	130.38	131.38	1.50	−1.48	11.36	this study
14	6	28	30	29	130.78	131.78	2.07	−1.41	42.86	this study
14	6	68	70	69	131.18	132.18	2.07	−0.88	65.17	this study
14	6	94	96	95	131.44	132.44	1.62	−1.82	64.99	this study
14	6	134	136	135	131.84	132.84	1.73	−1.29	73.04	this study

CPD
10, 3163–3221, 2014

Table 5. Continued.

Core	Section	Top (cm)	Bottom (cm)	Mid (cm)	mbsf	mcd	$\delta^{13}C$	$\delta^{18}O$	$CaCO_3$ (%)	Source
15	1	1	3	2	132.91	134.50			2.32	this study
15	1	10	12	11	133.00	134.60			1.78	this study
15	1	19.5	21.5	20.5	133.14	134.70	1.17	−0.76	2.47	this study
15	1	30	32	31	133.20	134.80			3.96	this study
15	1	40	42	41	133.30	134.90			2.25	this study
15	1	50	52	51	133.40	135.00	1.70	−1.00	6.70	this study
15	1	60	62	61	133.54	135.10	1.64	−2.49	5.60	this study
15	1	79	82	80.5	133.74	135.30	1.98	−1.07	7.35	this study
15	1	100	102	101	133.94	135.50	1.91	−1.63	6.98	this study
15	1	140	142	141	134.34	135.90	1.88	−1.34	20.64	this study
15	2	30	32	31	134.74	136.30	1.79	−2.17	35.64	this study
15	2	70	72	71	135.14	136.70	1.79	−1.16	61.67	this study
15	2	110	112	111	135.54	137.10	1.86	−1.13	60.70	this study
15	3	2	4	3	135.96	137.52	1.64	−1.19	57.02	this study
15	3	10	12	11	136.04	137.60	1.78	−0.83	74.17	this study
15	3	20	22	21	136.14	137.70	1.71	−1.14	37.85	this study
15	3	29	31	30	135.23	137.79	1.80	−0.90	44.48	this study
15	3	40	42	41	136.34	137.90	1.70	−1.23	78.59	this study
15	3	60	62	61	136.54	138.10	1.78	−0.96	88.50	this study
15	3	78	80	79	136.72	138.28	1.55	−1.74	84.68	this study
15	3	100	102	101	136.94	138.50	1.62	−0.90	81.52	this study
15	3	120	122	121	137.14	138.70	1.59	−0.96	83.79	this study
15	3	140	142	141	137.34	138.90	1.53	−0.80	78.87	this study
15	4	10	12	11	137.54	139.10	1.35	−1.49	26.22	this study
15	4	21	23	22	137.65	139.21	1.39	−1.09	76.66	this study
15	4	30	32	31	137.74	139.30	1.40	−1.51	58.17	this study
15	4	40.5	42.5	41.5	137.85	139.41	1.52	−1.06	85.08	this study
15	4	48.5	50.5	49.5	137.93	139.49	1.52	−1.02	81.43	this study
15	4	59	61	60	138.03	139.59	1.38	−2.05	74.96	this study
15	4	66	68	67	138.10	139.66	1.46	−1.31	70.16	this study
15	4	79	81	80	138.23	139.79	1.37	−1.16	39.51	this study
15	4	89	91	90	138.33	139.89	1.68	−1.57	83.35	this study
15	4	100.5	102.5	101.5	138.45	140.01	1.58	−1.69	83.20	this study
15	4	110	112	111	138.54	140.10	1.68	−0.96	85.29	this study
15	4	125	127	126	138.69	140.25	1.69	−1.07	70.98	this study
15	4	140	142	141	138.84	140.40	1.74	−1.19	86.34	this study
15	5	5	7	6	138.99	140.55	1.59	−1.21	87.08	this study
15	5	39.5	41.5	40.5	139.34	140.90	1.60	−2.16	84.88	this study
15	5	80	82	81	139.74	141.30	1.67	−1.37	86.53	this study
15	5	120	122	121	140.14	141.70	1.74	−1.30	86.78	this study
15	6	10	12	11	140.54	142.10	2.01	−0.95	90.13	this study
15	6	53	55	54	140.97	142.53	2.14	−1.52	90.93	this study
15	6	90	92	91	141.34	142.90	2.00	−1.32	88.69	this study

CPD
10, 3163–3221, 2014

Table 5. Continued.

Core	Section	Top (cm)	Bottom (cm)	Mid (cm)	mbsf	mcd	$\delta^{13}C$	$\delta^{18}O$	$CaCO_3$ (%)	Source
16	1	80	83	81.5	142.78	145.82	2.21	−1.08		Ravizza et al. (2001)
16	1	82	84	83	142.82	145.82	2.16	−1.19	91.23	this study
16	1	91	95	93	142.89	145.93	2.17	−1.10		Ravizza et al. (2001)
16	1	102	106	104	143.00	146.04	2.13	−1.10		Ravizza et al. (2001)
16	1	110	113	111.5	143.08	146.12	2.08	−1.15		Ravizza et al. (2001)
16	1	121	124	122.5	143.19	146.23	2.08	−1.19		Ravizza et al. (2001)
16	1	131	134	132.5	143.29	146.33	2.12	−1.18		Ravizza et al. (2001)
16	1	137	139	138	143.37	146.37	2.14	−1.25	85.34	this study
16	1	141	144	142.5	143.39	146.43	2.16	−1.01		Ravizza et al. (2001)
16	2	8	12	10	143.57	146.60	2.20	−1.07		Ravizza et al. (2001)
16	2	28	32	30	143.77	146.80	2.23	−0.94		Ravizza et al. (2001)
16	2	42	46	44	143.91	146.94	2.19	−0.93		Ravizza et al. (2001)
16	2	50	54	52	143.99	147.02	2.27			Ravizza et al. (2001)
16	2	61	65	63	144.10	147.13	2.10	−1.18		Ravizza et al. (2001)
16	2	65	67	66	144.15	147.15	2.18	−1.32	89.97	this study
16	2	69	73	71	144.18	147.21	2.25	−0.79		Ravizza et al. (2001)
16	2	80	84	82	144.29	147.32	2.21	−0.88		Ravizza et al. (2001)
16	2	90	94	92	144.39	147.42	2.22	−0.77		Ravizza et al. (2001)
16	2	100	104	102	144.49	147.52	2.20	−0.78		Ravizza et al. (2001)
16	2	111	115	113	144.60	147.63	2.17	−0.78		Ravizza et al. (2001)
16	2	120	124	122	144.69	147.72	2.18	−0.77		Ravizza et al. (2001)
16	2	130	134	132	144.79	147.82	2.19	−0.83		Ravizza et al. (2001)
16	2	139	141	140	144.89	147.89	2.09	−1.18	90.85	this study
16	2	140	144	142	144.89	147.92	2.17	−0.77		Ravizza et al. (2001)
16	3	0	4	2	144.98	148.02	2.16	−0.74		Ravizza et al. (2001)
16	3	15	19	17	145.13	148.17	2.14	−0.71		Ravizza et al. (2001)
16	3	22	26	24	145.20	148.24	2.14	−0.75		Ravizza et al. (2001)
16	3	32	36	34	145.30	148.34	2.14	−0.78		Ravizza et al. (2001)
16	3	42	46	44	145.40	148.44	2.03	−0.91		Ravizza et al. (2001)
16	3	52	56	54	145.50	148.54	2.02	−0.82		Ravizza et al. (2001)
16	3	62	66	64	145.60	148.64	2.07	−0.75		Ravizza et al. (2001)
16	3	67	69	68	145.67	148.67	2.10	−0.71	91.43	this study
16	3	80	84	82	145.78	148.82	2.10	−0.67		Ravizza et al. (2001)
16	3	91	95	93	145.89	148.93	2.08	−0.61		Ravizza et al. (2001)
16	3	100	104	102	145.98	149.02	2.04	−0.67		Ravizza et al. (2001)
16	3	111	115	113	146.09	149.13	2.06	−0.64		Ravizza et al. (2001)
16	3	121	125	123	146.19	149.23	2.05	−0.62		Ravizza et al. (2001)
16	3	131	135	133	146.29	149.33	2.03	−0.71		Ravizza et al. (2001)
16	3	133	135	134	146.33	149.33	2.04	−0.83	89.12	this study
16	4	7	8	7.5	146.55	149.55	2.02	−0.90	102.83	this study
16	4	10	14	12	146.58	149.62	1.99	−0.75		Ravizza et al. (2001)
16	4	20	24	22	146.68	149.72	1.95	−0.82		Ravizza et al. (2001)
16	4	31	35	33	146.79	149.83	1.96	−0.73		Ravizza et al. (2001)
16	4	40	44	42	146.88	149.92	1.92	−0.78		Ravizza et al. (2001)
16	4	50	51	50.5	146.98	149.98	1.73	−1.01	100.42	this study
16	4	50	54	52	146.98	150.02	1.63	−0.93		Ravizza et al. (2001)
16	4	61	65	63	147.09	150.13	1.60	−0.94		Ravizza et al. (2001)
16	4	71	75	73	147.19	150.23	1.72	−0.78		Ravizza et al. (2001)
16	4	81	85	83	147.29	150.33	1.40	−1.21		Ravizza et al. (2001)
16	4	91	95	93	147.39	150.43	1.42	−1.11		Ravizza et al. (2001)
16	4	101	105	103	147.49	150.53	1.10	−1.54		Ravizza et al. (2001)
16	4	111	115	113	147.59	150.63	1.05	−1.56		Ravizza et al. (2001)
16	4	122	126	124	147.70	150.74	0.92	−1.89		Ravizza et al. (2001)
16	4	130	134	132	147.78	150.82	0.83	−0.52		Ravizza et al. (2001)
16	4	135	136	135.5	147.83	150.83	0.69	−2.05	19.87	this study
16	4	135	136	135.5	147.83	150.83			19.75	this study
16	CC	N/A	N/A		148.18	151.18			2.74	this study

CPD
10, 3163–3221, 2014

Table 6. Site 214.

Core	Section	Top (cm)	Bottom (cm)	Mid (cm)	mbsf	mcd	$d^{13}C$	$d^{18}O$	CaCO3 (%)	Source
34	1	10	12	11	314.55	314.55	1.86	−0.51	91.89	this study
34	1	50	52	51	314.95	314.95	1.82	−0.29	93.22	this study
34	1	90	92	91	315.35	315.35	1.71	−0.74	93.21	this study
34	1	130	132	131	315.75	315.75	1.84	−0.49	92.84	this study
34	2	20	22	21	316.15	316.15	1.86	−0.38	95.03	this study
34	2	60	62	61	316.55	316.55	1.93	−0.44	92.73	this study
34	2	100	102	101	316.95	316.95	1.97	−0.35	92.03	this study
34	2	140	142	141	317.35	317.35	1.86	−0.42	93.88	this study
34	3	30	32	31	317.75	317.75	1.74	−0.51	93.51	this study
34	3	70	72	71	318.15	318.15	1.75	−0.71	93.45	this study
34	3	110	112	111	318.55	318.55	1.72	−0.52	93.28	this study
34	4	3	5	4	318.98	318.98	1.81	−0.56	93.30	this study
34	4	40	42	41	319.35	319.35	1.83	−0.58	93.05	this study
34	4	80	82	81	319.75	319.75	1.85	−0.48	91.98	this study
34	4	120	122	121	320.15	320.15	1.73	−0.89	93.43	this study
34	5	10	12	11	320.55	320.55	1.76	−0.52	92.86	this study
34	5	50	52	51	320.95	320.95	1.70	−0.66	93.78	this study
34	5	90	92	91	321.35	321.35	1.72	−0.61	92.99	this study
34	5	130	132	131	321.75	321.75	1.70	−0.68	92.26	this study
34	6	20	22	21	322.15	322.15	1.77	−0.62	92.80	this study
34	6	60	62	61	322.55	322.55	1.76	−0.67	92.89	this study
34	6	99	101	100	322.94	322.94	1.67	−0.75	93.34	this study
34	6	133.5	135.5	134.5	323.29	323.29	1.72	−0.84	92.02	this study
35	1	4	6	5	323.54	324.54	1.16	−0.97	92.93	this study
35	1	15	18	16.5	323.65	324.65	1.32	−0.85	90.53	this study
35	1	33	36	34.5	323.83	324.83	1.35	−0.85	90.17	this study
35	1	49	51	50	323.99	324.99	1.03	−0.88	91.16	this study
35	1	64	66	65	324.14	325.14	1.04	−0.97	90.74	this study
35	1	80	82	81	324.30	325.30	1.03	−0.92	90.07	this study
35	1	98	100	99	324.48	325.48	1.11	−0.77	91.36	this study
35	1	110	112	111	324.60	325.60	1.14	−0.84	90.10	this study
35	1	123.5	125.5	124.5	324.74	325.74	1.07	−1.03	90.48	this study
35	1	140	142	141	324.90	325.90	1.05	−0.84	89.97	this study
35	2	2	4	3	325.02	326.02	1.07	−0.79	91.17	this study
35	2	13	15	14	325.13	326.13	1.05	−1.22	89.10	this study
35	2	28	30	29	325.28	326.28	1.08	−0.85	87.49	this study
35	2	39	41	40	325.39	326.39	1.11	−0.79	87.31	this study
35	2	44	46	45	325.44	326.44	1.11	−0.92	88.00	this study
35	2	60	62	61	325.60	326.60	1.15	−0.86	86.98	this study
35	2	80	82	81	325.80	326.80	1.08	−0.87	86.28	this study
35	2	100	102	101	326.00	327.00	1.08	−0.85	85.25	this study
35	2	120	122	121	326.20	327.20	1.10	−0.90	85.80	this study
35	2	138	140	139	326.38	327.38	1.09	−0.86	85.90	this study
35	2	146	148	147	326.46	327.46	1.02	−0.91	86.21	this study
35	3	0	2	1	326.50	327.50	0.99	−1.07	87.96	this study
35	3	24	26	25	326.74	327.74	0.91	−0.83	86.85	this study
35	3	38	40	39	326.88	327.88	0.96	−0.94	86.75	this study

CPD
10, 3163–3221, 2014

Table 6. Continued.

Core	Section	Top (cm)	Bottom (cm)	Mid (cm)	mbsf	mcd	$\delta^{13}C$	$\delta^{18}O$	$CaCO_3$ (%)	Source
35	3	50	52	51	327.00	328.00	0.93	−0.81	87.55	this study
35	3	64	66	65	327.14	328.14	0.95	−0.82	87.53	this study
35	3	74	76	75	327.24	328.24	0.91	−0.83	85.59	this study
35	3	84	86	85	327.34	328.34	1.00	−0.76	87.01	this study
35	3	100	102	101	327.50	328.50	0.89	−0.83	88.35	this study
35	3	114	116	115	327.64	328.64	1.00	−0.94	88.79	this study
35	3	128	130	129	327.78	328.78	0.90	−0.80	86.78	this study
35	3	146	148	147	327.96	328.96	0.95	−0.77	87.91	this study
35	4	20	22	21	328.20	329.20	0.95	−0.79	85.83	this study
35	4	40	42	41	328.40	329.40	0.92	−1.21	87.83	this study
35	4	60	62	61	328.60	329.60	0.92	−1.25	84.70	this study
35	4	100	102	101	329.00	330.00	0.90	−0.77	81.53	this study
35	4	140	142	141	329.40	330.40	0.92	−1.40	75.99	this study
35	4	145	147	146	329.45	330.45	1.02	−0.87	76.20	this study
35	cc				329.74	330.74	1.09	−0.91	73.83	this study
36	1	109	111	110	334.09	336.09	0.63	0.11	50.19	this study
36	1	146	148	147	334.46	336.46	0.53	−0.01	41.29	this study
36	2	40	42	41	334.90	336.90	1.65	−0.82	20.65	this study
36	2	80	82	81	335.30	337.30	1.47	−0.59	21.09	this study
36	2	120	122	121	335.70	337.70	1.33	−1.00	20.18	this study
36	3	10	12	11	336.10	338.10	1.28	−0.60	22.99	this study
36	3	50	52	51	336.50	338.50	1.27	−0.52	21.29	this study
36	3	90	92	91	336.90	338.90	1.40	−0.49	18.32	this study
36	3	128	130	129	337.28	339.28	1.46	−0.69	19.89	this study
36	4	20	22	21	337.70	339.70	1.39	−0.52	19.97	this study
36	4	60	62	61	338.10	340.10	0.31	−0.65	22.52	this study
36	4	100	102	101	338.50	340.50	0.93	−0.48	17.68	this study
36	4	136	138	137	338.86	340.86	0.24	−0.51	44.49	this study
37	1	11	13	12	342.61	345.61	1.16	−0.47	21.00	this study
37	1	52	54	53	343.02	346.02	0.08	−0.32	64.75	this study
37	1	90	92	91	343.40	346.40	0.87	−0.09	51.52	this study
37	1	130	132	131	343.80	346.80	0.85	−0.50	47.97	this study
37	2	20	22	21	344.20	347.20	0.92	−0.19	46.12	this study
37	2	60	62	61	344.60	347.60	0.94	−0.11	47.54	this study
37	2	100	102	101	345.00	348.00	0.84	−0.20	53.50	this study
37	2	138	140	139	345.38	348.38	0.69	−0.42	62.72	this study
38	1	109	111	110	353.09	357.09	−0.84	−0.51	60.50	this study
38	2	40	42	41	353.90	357.90	−0.62	−0.53	48.52	this study
38	2	80	82	81	354.30	358.30	−0.78	−0.26	43.46	this study
38	2	120	122	121	354.70	358.70	−0.57	−0.55	56.91	this study
38	3	8.5	10.5	9.5	355.09	359.09	0.26	−0.58	49.43	this study
38	3	51	52	51.5	355.51	359.51	−0.74	−0.34	53.13	this study
38	3	91	92	91.5	355.91	359.91	−0.06	−0.27	56.60	this study
38	3	130	132	131	356.30	360.30	−0.86	−0.61	52.46	this study
38	4	20	22	21	356.70	360.70	−1.28	−0.75	47.05	this study
38	4	60	62	61	357.10	361.10	−0.73	−0.33	45.62	this study
38	4	97.5	99.5	98.5	357.48	361.48	−0.39	−0.72	45.49	this study
38	4	140	142	141	357.90	361.90	−1.84	−0.58	40.73	this study
39	1	113.5	115.5	114.5	362.64	367.64	1.60	−1.41	38.52	this study
39	2	2	4	3	363.02	368.02	−1.88	−1.03	38.53	this study
39	2	37.5	39.5	38.5	363.38	368.38	−2.89	−0.39	37.00	this study
39	2	80	82	81	363.80	368.80	−2.32	−0.69	22.47	this study
39	2	120	122	121	364.20	369.20	−3.09	−1.33	18.50	this study
39	3	9.5	11.5	10.5	364.60	369.60	−4.34	−1.42	14.40	this study
39	3	50	52	51	365.00	370.00	−5.90	−0.88	20.98	this study
39	3	90	92	91	365.40	370.40	−5.16	−1.52	12.51	this study
39	3	130	132	131	365.80	370.80	−2.36	−0.60	4.14	this study

CPD
10, 3163–3221, 2014

Table 7. Site 215.

Core	Section	Top (cm)	Bottom (cm)	Mid (cm)	mbsf	mcd	d13C	d18O	CaCO3 (%)	Source
8	1	87	89	88	65.37	65.37			1.42	this study
8	1	134	136	135	65.84	65.84			1.22	this study
8	2	54	56	55	66.54	66.54			1.45	this study
8	2	124	126	125	67.24	67.24			2.40	this study
8	3	52	54	53	68.02	68.02			1.35	this study
8	3	130	132	131	68.80	68.80			1.05	this study
8	4	29	31	30	69.29	69.29			1.43	this study
8	4	117	119	118	70.17	70.17			1.19	this study
8	5	74	76	75	71.24	71.24			1.30	this study
9	1	29	31	30	74.29	75.29			1.17	this study
9	1	60	62	61	74.60	75.60			2.04	this study
9	1	100	102	101	75.00	76.00			1.26	this study
9	1	140	142	141	75.40	76.40			0.96	this study
9	2	30	32	31	75.80	76.80			1.56	this study
9	2	70	72	71	76.20	77.20			1.38	this study
9	2	110	112	111	76.60	77.60			1.51	this study
9	3	5	7	6	77.05	78.05			1.35	this study
9	3	21	23	22	77.21	78.21			1.21	this study
9	3	40	42	41	77.40	78.40			1.24	this study
9	3	60	62	61	77.60	78.60			1.33	this study
9	3	82	84	83	77.82	78.82	2.00	−0.75	13.64	this study
9	3	105	107	106	78.05	79.05	2.03	−1.21	65.70	this study
9	3	120	122	121	78.20	79.20	1.97	−0.57	65.34	this study
9	3	140	142	141	78.40	79.40	1.71	−1.41	76.47	this study
10	1	110	112	111	84.60	86.60	1.08	−0.73	87.79	this study
10	1	120	122	121	84.70	86.70	1.26	−1.34	85.03	this study
10	1	130.5	132.5	131.5	84.81	86.81	1.36	−0.82	83.51	this study
10	1	140	142	141	84.90	86.90	1.21	−0.82	84.42	this study
10	2	10	12	11	85.10	87.10	1.30	−1.43	86.43	this study
10	2	32	34	33	85.32	87.32	1.33	−1.67	91.32	this study
10	2	47	49	48	85.47	87.47	1.44	−0.56	91.03	this study
10	2	70	72	71	85.70	87.70	1.40	−0.63	90.34	this study
10	2	90	92	91	85.90	87.90	1.40	−1.22	93.40	this study
10	2	108	110	109	86.08	88.08	1.32	−0.61	89.09	this study
10	2	129	131	130	86.29	88.29	1.19	−0.82	91.19	this study
10	3	27	29	28	86.77	88.77	1.47	−0.88	93.07	this study
10	3	40.0	42	41	86.90	88.90	1.43	−1.07	92.42	this study
10	3	60	62	61	87.10	89.10	1.43	−0.86	90.33	this study
10	3	80	82	81	87.30	89.30	1.48	−0.80	87.27	this study
10	3	100	102	101	87.50	89.50	1.63	−0.73	90.17	this study
10	3	118	120	119	87.68	89.68	1.37	0.15	88.33	this study
10	3	140	142	141	87.90	89.90	1.66	−0.85	89.33	this study
11	1	21	23	22	93.21	96.21	1.90	−0.65	91.46	this study
11	1	40	42	41	93.40	96.40	1.82	−0.63	89.43	this study
11	1	60	62	61	93.60	96.60	1.91	−0.64	86.79	this study
11	1	79.0	81	80	93.79	96.79	1.88	−1.15	88.65	this study
11	1	79	81	80	93.79	96.79	1.91	−0.64	89.92	this study
11	1	100	102	101	94.00	97.00	1.89	−0.90	86.12	this study
11	1	120	122	121	94.20	97.20	1.88	−0.64	88.14	this study
11	1	140	142	141	94.40	97.40	1.87	−0.94	90.98	this study
11	2	3	5	4	94.53	97.53	1.87	−0.72	89.78	this study
11	2	20	22	21	94.70	97.70	1.87	−1.11	89.12	this study
11	2	50	52	51	95.00	98.00	1.88	−1.29	92.38	this study
11	2	80	82	81	95.30	98.30	1.91	−0.78	88.73	this study
11	2	107	109	108	95.57	98.57	2.35	−1.78	86.69	this study
11	2	138	140	139	95.88	98.88	1.91	−0.79	89.98	this study
11	3	22	24	23	96.22	99.22	1.93	−0.53	91.52	this study
11	3	50	52	51	96.50	99.50	1.93	−0.98	90.09	this study
11	3	78	80	79	96.78	99.78	1.93	−1.13	91.18	this study
11	3	110	112	111	97.10	100.10	1.94	−1.12	88.73	this study

CPD
10, 3163–3221, 2014

Table 7. Continued.

Core	Section	Top (cm)	Bottom (cm)	Mid (cm)	mbsf	mcd	$\delta^{13}C$	$\delta^{18}O$	$CaCO_3$ (%)	Source
11	3	140	142	141	97.40	100.40	1.88	−0.75	91.36	this study
11	4	19	21	20	97.69	100.69	2.04	−0.92	90.22	this study
11	4	48	50	49	97.98	100.98	1.83	−2.09	90.67	this study
11	4	80	82	81	98.30	101.30	1.74	−0.72	92.18	this study
11	4	110	112	111	98.60	101.60	2.04	−0.85	90.51	this study
11	4	140	142	141	98.90	101.90	2.01	−0.63	92.18	this study
11	5	20	22	21	99.20	102.20	2.06	−0.68	91.08	this study
11	5	48	50	49	99.48	102.48	1.85	−1.36	90.08	this study
11	5	77.5	79.5	78.5	99.78	102.78	1.88	−0.75	90.32	this study
11	5	110	112	111	100.10	103.10	1.89	−1.05	93.23	this study
11	5	130.5	132.5	131.5	100.31	103.31	1.86	−1.10	96.58	this study
11	6	18	20	19	100.68	103.68	2.55	1.31	90.33	this study
11	6	49	51	50	100.99	103.99	1.89	−1.20	92.03	this study
11	6	77	79	78	101.27	104.27	1.80	−0.77	92.65	this study
11	6	108	110	109	101.58	104.58	2.02	−0.52	92.38	this study
11	6	137.5	139.5	138.5	101.88	104.88	1.77	−1.36	86.63	this study
12	1	20	22	21	102.70	106.70	1.91	−0.61	89.81	this study
12	1	40	42	41	102.90	106.90	2.25	−0.87	87.61	this study
12	1	60	62	61	103.10	107.10	2.56	−0.73	88.14	this study
12	1	77	79	78	103.27	107.27	2.53	−0.67	90.57	this study
12	1	87	89	88	103.37	107.37	2.30	−1.57	89.15	this study
12	1	97	99	98	103.47	107.47	2.33	−0.79	88.05	this study
12	1	107	109	108	103.57	107.57	2.22	−0.70	90.21	this study
12	1	115	117	116	103.65	107.65	2.51	−0.55	90.04	this study
12	1	127	129	128	103.77	107.77	2.38	−0.65	94.68	this study
12	1	136	138	137	103.86	107.86	2.21	−0.92	90.53	this study
12	2	2	4	3	104.02	108.02	2.34	−0.93	89.12	this study
12	2	10	12	11	104.10	108.10	2.20	−0.72	89.33	this study
12	2	20	22	21	104.20	108.20	2.28	−1.03	88.00	this study
12	2	30	32	31	104.30	108.30	2.27	−0.70	87.24	this study
12	2	40	42	41	104.40	108.40	2.13	0.33	87.23	this study
12	2	48	50	49	104.48	108.48	2.37	−0.55	92.66	this study
12	2	60	62	61	104.60	108.60	2.37	−0.62	88.58	this study
12	2	70	72	71	104.70	108.70	2.37	−0.70	88.41	this study
12	2	80	82	81	104.80	108.80	2.25	−0.81	87.81	this study
12	2	90	92	91	104.90	108.90	2.17	−0.70	85.22	this study
12	2	100	102	101	105.00	109.00	2.19	−0.77	83.54	this study
12	2	110.0	112	111	105.10	109.10	2.44	−0.62	89.32	this study
12	2	120	122	121	105.20	109.20	2.10	−0.65	90.54	this study
12	2	130	132	131	105.30	109.30	2.06	−0.66	89.40	this study
12	2	140	142	141	105.40	109.40	2.43	−0.87	88.04	this study
12	3	20	22	21	105.70	109.70	2.27	−0.63	87.21	this study
12	3	51	53	52	106.01	110.01	2.48	−0.54	88.85	this study
12	3	80	82	81	106.30	110.30	2.47	−0.64	88.49	this study
12	3	110	112	111	106.60	110.60	2.55	−0.58	90.00	this study
12	3	140	142	141	106.90	110.90	2.59	−0.56	89.37	this study
12	4	20	22	21	107.20	111.20	2.60	−1.11	89.18	this study
12	4	50	52	51	107.50	111.50	2.49	−1.68	91.22	this study
12	4	77	79	78	107.77	111.77	2.65	−1.30	90.04	this study
12	4	108	110	109	108.08	112.08	2.78	−0.76	90.78	this study
12	4	140	142	141	108.40	112.40	2.54	−0.55	91.62	this study
12	5	20	22	21	108.70	112.70	2.59	−0.62	91.09	this study
12	5	50	52	51	109.00	113.00	2.26	−0.66	90.06	this study
12	5	80	82	81	109.30	113.30	2.81	−0.40	89.48	this study
12	5	110	112	111	109.60	113.60	2.81	−0.51	91.50	this study
12	5	141	143	142	109.91	113.91	2.79	−0.53	91.24	this study
12	6	20	22	21	110.20	114.20	2.79	−1.05	92.43	this study
12	6	52	54	53	110.52	114.52	2.65	−1.06	90.42	this study

CPD
10, 3163–3221, 2014

Table 7. Continued.

Core	Section	Top (cm)	Bottom (cm)	Mid (cm)	mbsf	mcd	$\delta^{13}C$	$\delta^{18}O$	$CaCO_3$ (%)	Source
12	6	80	82	81	110.80	114.80	2.77	−0.62	91.45	this study
12	6	110	112	111	111.10	115.10	2.64	−0.96	91.76	this study
12	6	140	142	141	111.40	115.40	2.73	−0.80	87.77	this study
13	1	118	120	119	113.18	118.18	3.20	−0.61	90.93	this study
13	1	134	136	135	113.34	118.34	3.35	−1.08	90.63	this study
13	1	134	136	135	113.34	118.34	3.07	−0.62	90.77	this study
13	1	142	144	143	113.42	118.42	3.41	−0.45	94.19	this study
13	2	2	4	3	113.53	118.53	3.45	−0.44	93.08	this study
13	2	12.5	14.5	13.5	113.64	118.64	3.60	−0.47	91.71	this study
13	2	22	24	23	113.73	118.73	3.62	−0.39	93.05	this study
13	2	30.5	32.5	31.5	113.82	118.82	3.36	−0.47	93.09	this study
13	2	42	44	43	113.93	118.93	3.26	−0.49	91.94	this study
13	2	52	54	53	114.03	119.03	3.22	−0.90	90.41	this study
13	2	62	64	63	114.13	119.13	3.22	−0.72	89.26	this study
13	2	72	74	73	114.23	119.23	2.95	−1.72	89.47	this study
13	2	82.5	84.5	83.5	114.34	119.34	2.75	−2.01	85.98	this study
13	2	92	94	93	114.43	119.43	3.00	−0.58	86.62	this study
13	2	92	94	93	114.43	119.43	3.00	−0.66	85.41	this study
13	2	112	114	113	114.63	119.63	2.92	−0.71	81.67	this study
13	2	122	124	123	114.73	119.73	3.20	−0.64	87.06	this study
13	2	132	134	133	114.83	119.83	3.16	−1.07	88.03	this study
13	2	142	144	143	114.93	119.93	3.32	−0.54	88.88	this study
13	3	2	4	3	115.03	120.03	2.89	0.59	86.11	this study
13	3	12	14	13	115.13	120.13	3.21	−1.05	87.83	this study
13	3	22	24	23	115.23	120.23	3.23	−0.59	87.13	this study
13	3	32	34	33	115.33	120.33	3.26	−0.77	85.50	this study
13	3	32	34	33	115.33	120.33	3.12	−0.63	87.04	this study
13	3	42	44	43	115.43	120.43	2.97	−0.58	87.10	this study
13	3	52	54	53	115.53	120.53	3.29	−0.67	84.25	this study
13	3	62	64	63	115.63	120.63	3.25	−0.54	87.72	this study
13	3	72	74	73	115.73	120.73	3.24	−0.47	88.78	this study
13	3	82	84	83	115.83	120.83	3.38	−1.02	87.89	this study
13	3	99	101	100	116.00	121.00	3.37	−0.57	85.23	this study
13	3	99	101	100	116.00	121.00	3.27	−0.48	89.66	this study
13	3	109	111	110	116.10	121.10	3.42	−0.53	86.90	this study
13	3	119	121	120	116.20	121.20	3.35	−1.28	88.83	this study
13	3	128	130	129	116.29	121.29	3.45	−0.41	88.18	this study
13	4	3	5	4	116.54	121.54	3.44	−0.86	90.44	this study
13	4	13	15	14	116.64	121.64	3.71	−0.30	89.93	this study
13	4	23	25	24	116.74	121.74	3.23	−1.78	88.89	this study
13	4	33	35	34	116.84	121.84	3.47	−0.67	89.71	this study
13	4	43	45	44	116.94	121.94	3.43	−0.53	88.63	this study
13	4	53	55	54	117.04	122.04	3.57	−0.45	87.31	this study
13	4	63	65	64	117.14	122.14	3.36	−0.57	88.77	this study
13	4	73	75	74	117.24	122.24	3.54	−0.34	88.74	this study
13	4	93	95	94	117.44	122.44	3.44	−0.50	87.85	this study
13	4	103	105	104	117.54	122.54	3.41	−1.39	90.25	this study
13	4	121	123	122	117.72	122.72	3.38	−0.59	89.80	this study
13	4	143	145	144	117.94	122.94	3.14	−1.85	89.68	this study

CPD
10, 3163–3221, 2014

Table 7. Continued.

Core	Section	Top (cm)	Bottom (cm)	Mid (cm)	mbsf	mcd	$\delta^{13}C$	$\delta^{18}O$	$CaCO_3$ (%)	Source
14	1	14	16	15	121.64	127.64	3.52	−1.26	91.23	this study
14	1	53.5	55.5	54.5	122.04	128.04	3.23	−1.11	89.18	this study
14	1	53.5	55.5	54.5	122.04	128.04	3.28	−0.58	89.78	this study
14	1	90	92	91	122.40	128.40	3.34	−0.41	91.62	this study
14	1	127	129	128	122.77	128.77	3.33	−1.17	90.53	this study
14	2	17.5	19.5	18.5	123.18	129.18	3.24	−0.33	86.99	this study
14	2	58.5	60.5	59.5	123.59	129.59	3.25	−1.60	93.32	this study
14	2	102	104	103	124.02	130.02	3.54	−0.26	89.41	this study
14	2	142	144	143	124.42	130.42	3.19	−1.67	91.23	this study
14	3	27.5	29.5	28.5	124.78	130.78	3.43	−0.22	88.14	this study
14	3	70	72	71	125.20	131.20	3.35	−0.76	92.03	this study
14	3	110	112	111	125.60	131.60	3.48	−0.13	91.30	this study
14	4	2	4	3	126.02	132.02	3.14	−0.10	91.29	this study
14	4	39.5	41.5	40.5	126.40	132.40	3.17	−0.03	91.91	this study
14	4	80	82	81	126.80	132.80	3.15	−0.34	91.50	this study
14	4	119	121	120	127.19	133.19	3.07	−0.63	92.37	this study
14	5	10	12	11	127.60	133.60	3.19	−0.47	93.09	this study
14	5	47	49	48	127.97	133.97	3.38	−0.43	93.47	this study
14	5	90	92	91	128.40	134.40	3.23	−0.39	93.93	this study
14	5	130	132	131	128.80	134.80	2.24	0.80	90.41	this study
14	6	21.5	23.5	22.5	129.22	135.22	3.07	−1.10	92.21	this study
14	6	60	62	61	129.60	135.60	2.98	−0.71	92.01	this study
14	6	100	102	101	130.00	136.00	2.88	−0.52	94.14	this study
14	6	140	142	141	130.40	136.40	3.19	−1.64	90.79	this study

CPD
10, 3163–3221, 2014

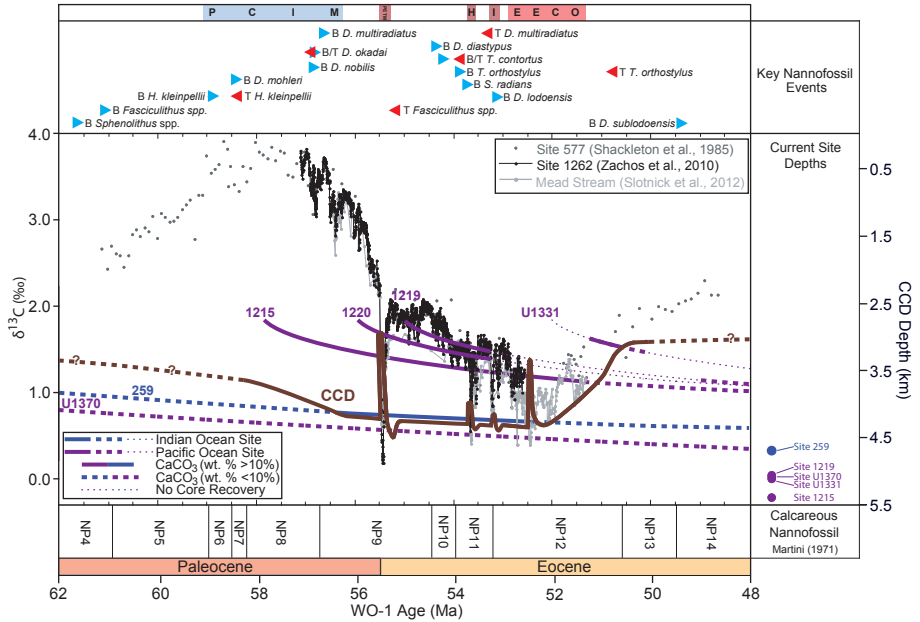

Figure 1. Bulk carbonate $\delta^{13}C$ records and calcareous intervals for several locations placed onto a current time scale (Option 1, Westerhold et al., 2008). Stable isotope records include those at DSDP Site 577 (North Pacific, Shackleton et al., 1985), ODP Site 1262 (Central Atlantic, Zachos et al., 2010) and Mead Stream (South Pacific, Slotnick et al., 2012). The subsidence curve for Site 259 (East Indian, blue) was adapted from (van Andel, 1975), while subsidence curves for Sites 1215, U1370, U1331, 1219, and 1220 (Equatorial Pacific, purple) were adapted from various sources (Rea and Lyle, 2005; Leon-Rodriguez et al., 2010; Pälike et al., 2010). Plotted curves, when solid, indicate carbonate contents > 10 %, but when dashed, indicate carbonate contents < 10 %. Importantly, curves are lightly dotted when no data is available (such as for much of the early Eocene at Sites 1219 and 1221, as noted by Hancock et al., 2007). Calcareous Nannofossil biozones are taken from Martini (1971), but adjusted to the current time scale.

CPD
10, 3163–3221, 2014

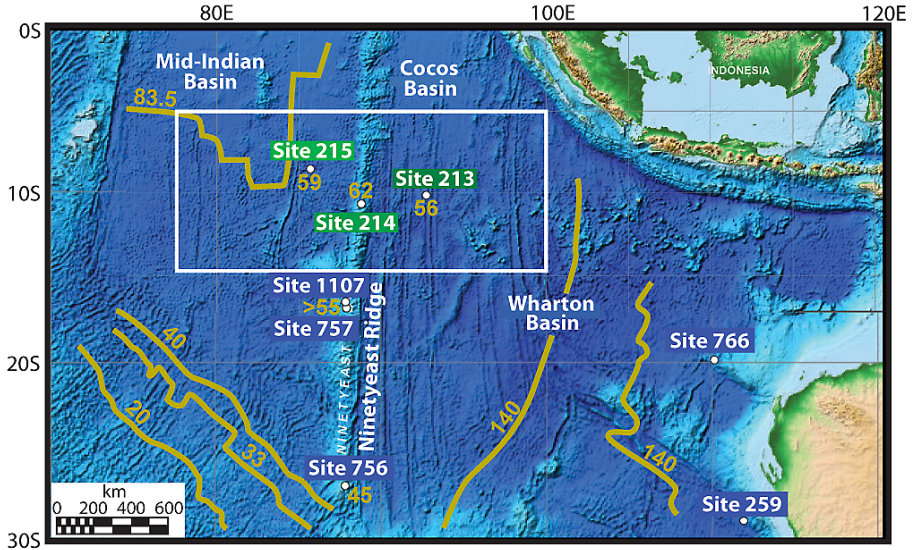

Figure 2. Modern bathymetric map of the northeast Indian Ocean. Locations of Sites 213, 214, 215 labeled in various shades of green. Five additional site locations are denoted in blue boxes along the western and northwest Australian margin (DSDP Site 259 – Hancock et al., 2007; ODP Site 766 – Shipboard Scientific Party, 1990), and Ninetyeast Ridge (ODP Sites 756 and 757 – Shipboard Scientific Party, 1989a, 1989b; ODP Site 1107 – Shipboard Scientific Party, 1999). Ages marked along Ninetyeast Ridge derived from Frey et al. (2011). All ages marked by green numbers follow a Myr time scale. The open white rectangle indicates the specific area of focus.

CPD
10, 3163–3221, 2014

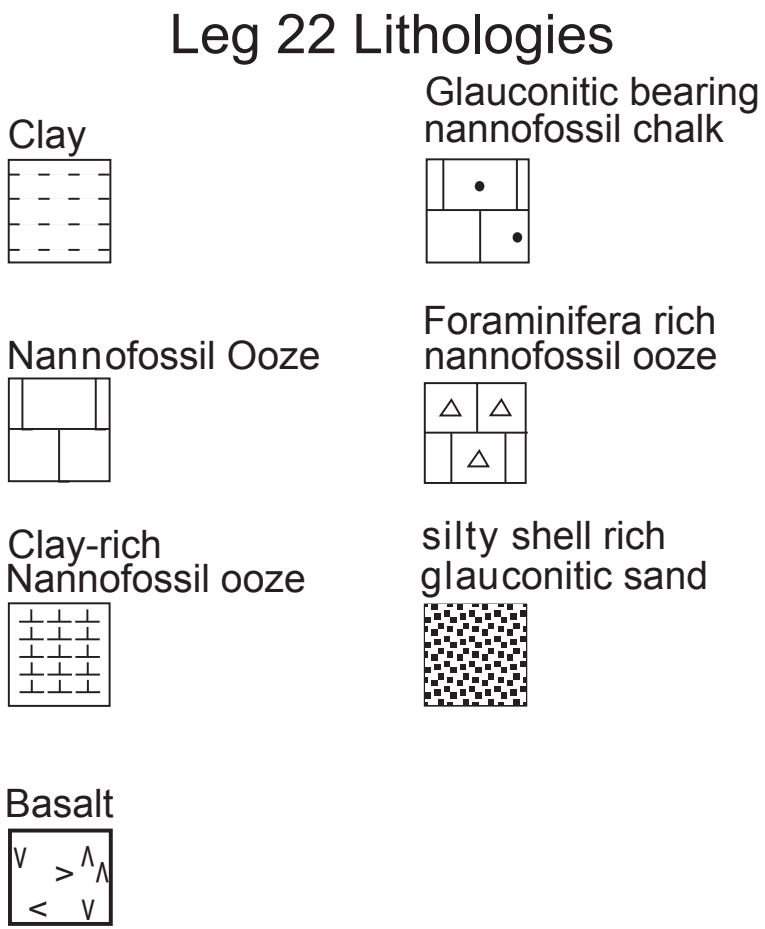

Figure 3. Lithological facies of core sections examined in this study.

CPD
10, 3163–3221, 2014

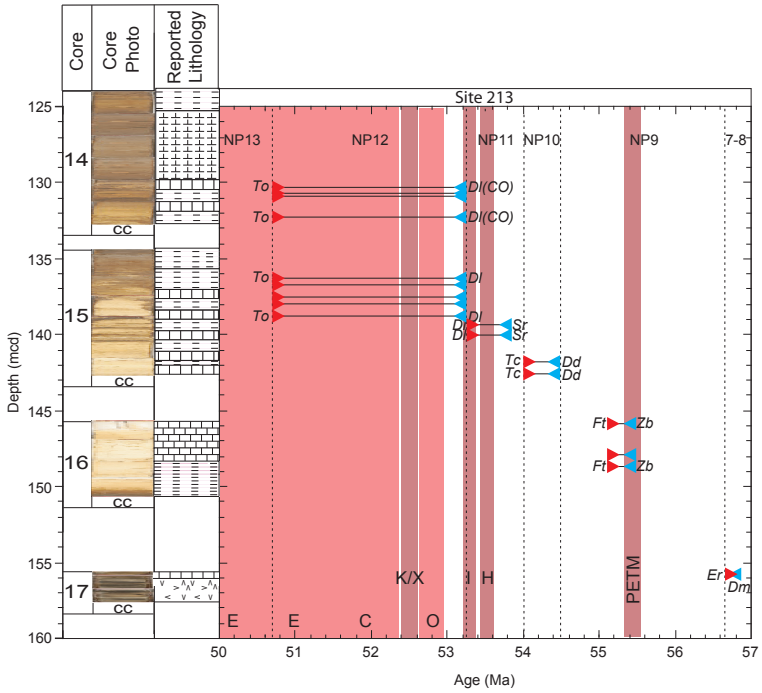

Figure 4. The depths of key nannofossil datums (bases – blue triangles, tops – red triangles) identified at Site 213. To and DI indicate presence of both *T. orthostylus* and *D. lodoensis*. DI and Sr indicate absence of *D. lodensis* and presence of *S. radians*. To and Dd indicate presence both of *T. orthostylus* and *D. diastypus*. Three samples marked Ft and Zb shows presence of both *F. tympaniformis* and *Z. bijugatus*, and dominance in abundance of *Z. bijugatus* over *F. tympaniformis*. Dm and Er indicate absence of *D. multiradiatus* and presence of *E. robusta*, according to Gartner (1974); data derived from sediment coated on basalt. Age estimates derived from Agnini et al. (2006, 2007) and calcareous nannofossil NP biozones from Martini (1971).

CPD
10, 3163–3221, 2014

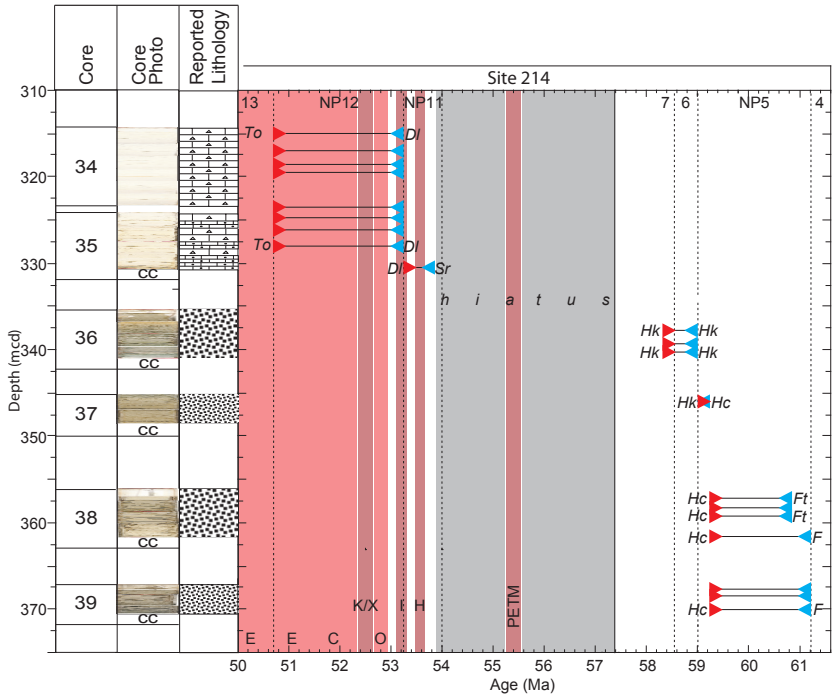

Figure 5. The depths of key nannofossil datums (bases – blue triangles, tops – red triangles) identified at Site 214. To and DI indicate presence of both *T. orthostylus* and *D. lodoensis*. DI and Sr indicate absence of *D. lodoensis* and presence of *S. radians*. Hk indicates presence of *H. kleinpellii*. Hk and Hc indicate absence of *H. kleinpellii* and presence of *H. cantabriae*. Hc and Ft indicate absence of *H. cantabriae* and presence of *F. tympaniformis*. Hc and F indicate absence of *H. cantabriae* and presence of *Fasciculithus* spp. (poor preservation only permit recognition at the genus level). Age estimates derived from Agnini et al. (2006, 2007) and calcareous nannofossil NP biozones from Martini (1971).

CPD
10, 3163–3221, 2014

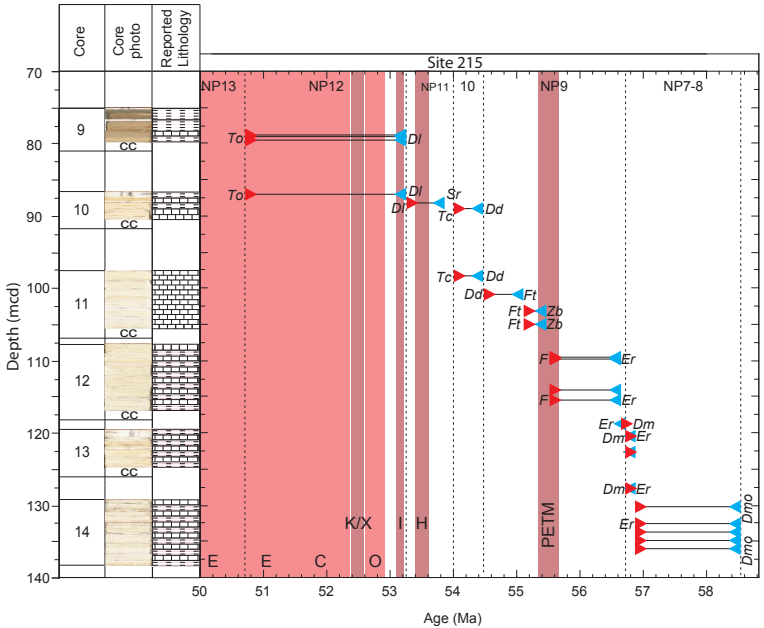

Figure 6. The depths of key nannofossil datums (bases – blue triangles, tops – red triangles) identified at Site 215. To and Dl indicate presence of both *T. orthostylus* and *D. lodoensis*. Dl and Sr indicate absence of *D. lodoensis* and presence of *S. radians*. Tc and Dd indicate presence of both *T. contortus* and *D. diastypus*. Dd and Ft indicate absence of *D. diastypus* and presence of few to rare *F. tympaniformis*. The two samples marked Ft and Zb indicates presence of both *F. tympaniformis* and *Z. bijugatus*, and dominance in abundance of *Z. bijugatus* over *F. tympaniformis*. The four samples marked F and Er shows presence of diverse and abundant *Fasciculithus* spp. and absence of *E. robusta*. Er and Dm indicate presence of both *E. robusta* and *D. multiradiatus*. Dm and Er indicate absence of *D. multiradiatus* and presence of *E. robusta*. The five samples marked Er and Dmo indicate absence of *E. robusta* and presence of *D. mohleri*. Age estimates derived from Agnini et al. (2006, 2007) and calcareous nannofossil NP biozones from Martini (1971).

CPD
10, 3163–3221, 2014

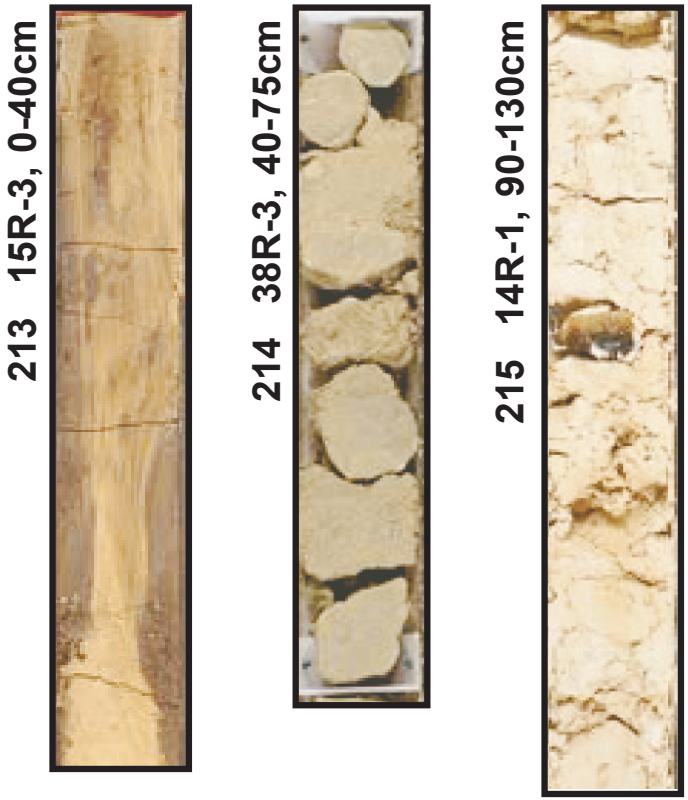

Figure 7. Core photos of disturbed sediment intervals recovered at each of the sites examined. When drilled in 1972, the sites were cored using rotary methods. As a result, there is considerable drilling disturbance over certain intervals.

CPD
10, 3163–3221, 2014

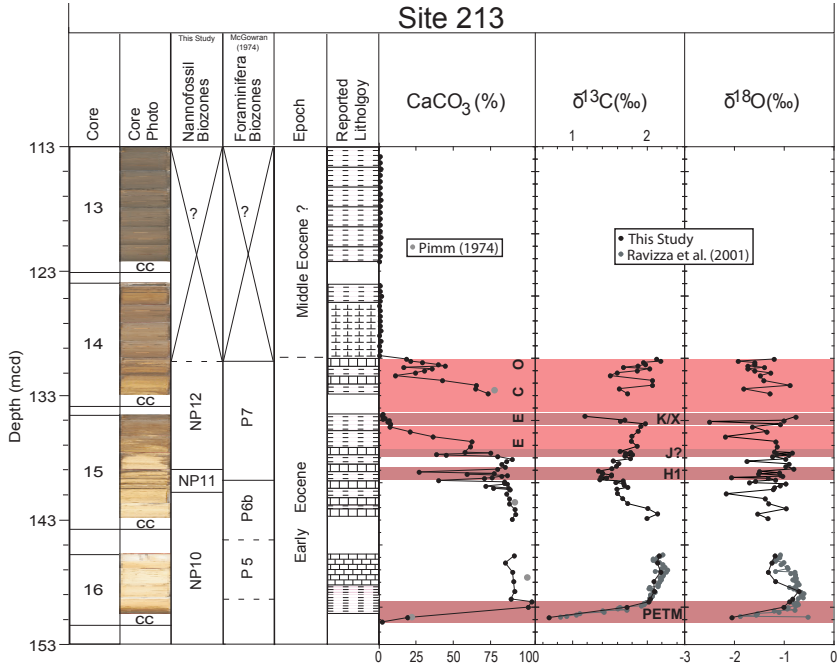

Figure 8. Early Paleogene sequences at DSDP Site 213. Biostratigraphy and lithology have been modified from the DSDP Leg 22 volume (von der Borch and Sclater, 1974). Core photos are sourced from the online database (www.iodp.org). Bulk carbonate $\delta^{13}C$ and $\delta^{18}O$ records near the base of Core 16 include data from previous work spanning the PETM recovery (grey – Ravizza et al., 2001). Carbonate content records include data from previous work (grey – Pimm, 1974). Consistent with the K/X-event occurring near the NP11/NP12 zonal boundary (Agnini et al., 2007), the H, J, and onset of K/X events occur in Core 15 sections 15-4, 15-3, and 15-1, respectively. The H and I events may have been mixed together since rotary coring was used for core collection. The upper portion of core 15 and all of core 14 likely spans the EECO, as indicated by depleted $\delta^{13}C$ and key zonal boundaries.

CPD
10, 3163–3221, 2014

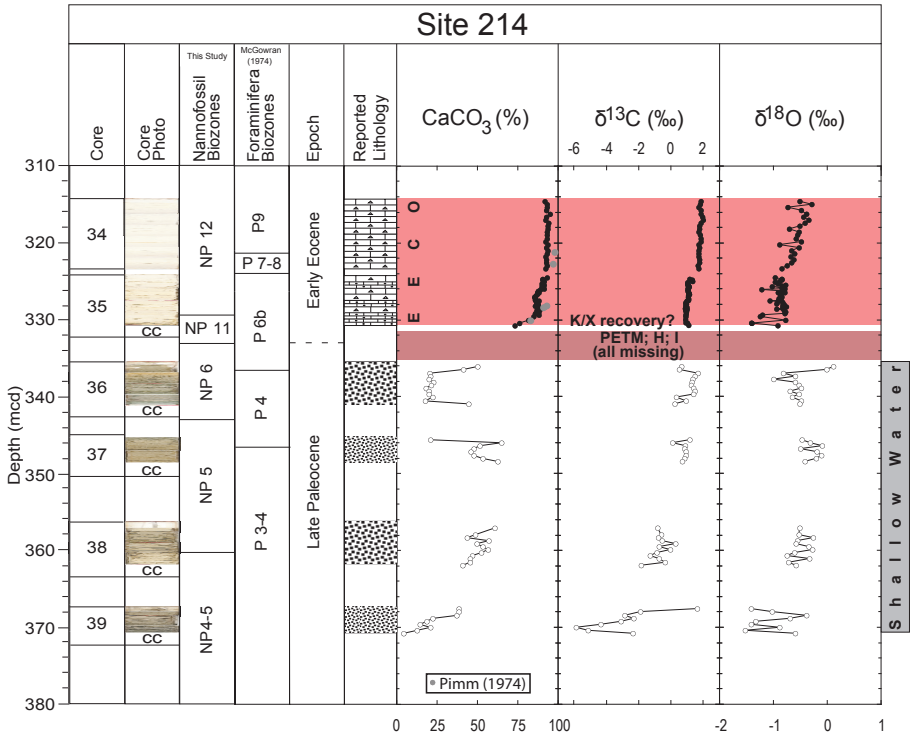

Figure 9. Early Paleogene sequences at DSDP Site 214. Biostratigraphy and lithology have been modified from the DSDP Leg 22 volume (von der Borch and Sclater, 1974). Core photos are sourced from the online database (www.iodp.org). Carbonate content records include data from previous work (grey – Pimm, 1974). Numerous hyperthermals, including the PETM, H events, I events, and K/X, are missing in the hiatus in the core gap between cores 36-35. It is possible that the uppermost recovery interval of the K/X-event spans the base of core 35 where already elevated carbonate contents increase slightly.

CPD
10, 3163–3221, 2014

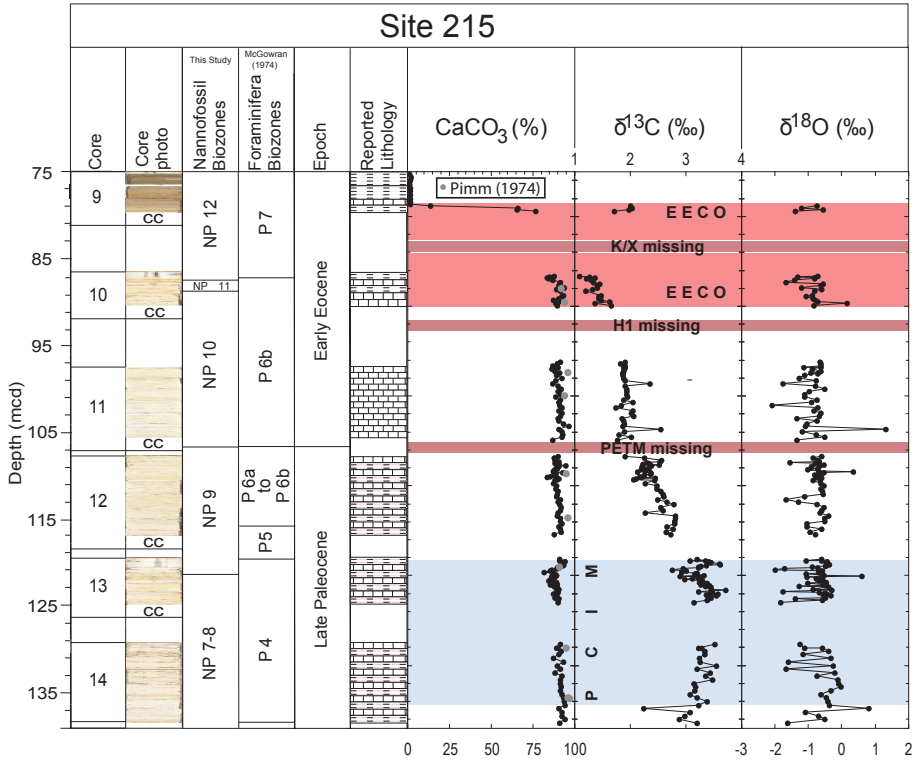

Figure 10. Early Paleogene sequences at DSDP Site 215. Biostratigraphy and lithology have been modified from the DSDP Leg 22 volume (von der Borch and Sclater, 1974). Core photos are sourced from the online database (www.iodp.org). Carbonate content records include data from previous work (grey – Pimm, 1974). Enriched $\delta^{13}C$ and biozonations enabled the identification of the PCIM in cores 14-13. The PETM is in the core gap between cores 12-11, consistent with the presence of the P5 foraminiferal biozone. The H events are in the core gap between cores 11-10. The NP10, NP11, and NP12 biozones and depleted $\delta^{13}C$ enabled the EECO identification in core 10. The K/X event is in the core gap between cores 10-9.

CPD
10, 3163–3221, 2014

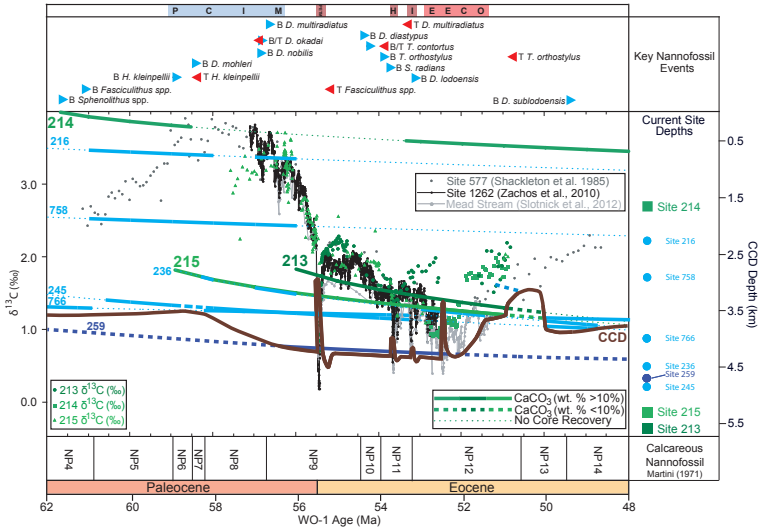

Figure 11. Bulk carbonate ^{13}C records and calcareous intervals for several locations placed onto a current time scale (Option 1, Westerhold et al., 2008). Stable isotope records include those at DSDP Site 577 (North Pacific, Shackleton et al., 1985), ODP Site 1262 (Central Atlantic, Zachos et al., 2010) and Mead Stream (South Pacific, Slotnick et al., 2012). Subsidence curves for Sites 213 and 215 (various shades of green) and for Sites 236, 245, and 766 (Shipboard Scientific Party, 1974b; Shipboard Scientific Party, 1974c; Shipboard Scientific Party, 1990, light blue) were calculated using a slightly modified version of the mid-ocean ridge subsidence curve from Rea and Lyle (2005). Subsidence curves for Site 214 (green) and for Sites 216 and 758 (Shipboard Scientific Party, 1974a; Shipboard Scientific Party, 1989c, light blue) follow established guidelines for aseismic ridges (Detrick et al., 1977). Plotted curves, when solid, indicate carbonate contents > 10 %, but when dashed, indicate carbonate contents < 10 %. Importantly, curves are lightly dotted when no data is available. Dark brown solid line denotes reconstructed CCD following new carbonate content data. Calcareous Nannofossil biozones are taken from Martini (1971), but adjusted to the current time scale.

CPD
10, 3163–3221, 2014

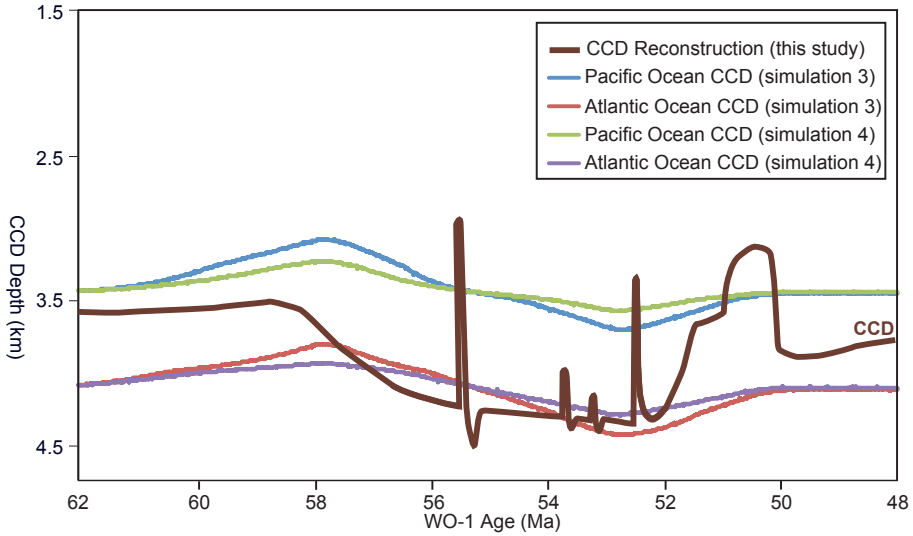

Figure 12. Comparison of data-derived-CCD changes (brown; this study) to modeled CCD changes predicted for the Atlantic and Pacific Oceans (green, purple, blue, and red) from 62–48 Ma (Komar et al., 2013). Records and models indicate a long-term (> 1 Myr) CCD deepening from 58–52 Ma separated two intervals of CCD shoaling from 62–58 Ma and 52–48 Ma. CCD curves have different magnitudes, by several hundreds of meters, suggesting the overall carbon cycling framework is correct but with a major caveat; either mass flux variations in the modeling are too small, or CCD depth constraints require additional characterization.

CPD
10, 3163–3221, 2014